Characterization of Calcite Amygdules in Devonian Basalts, in the McArras Brook Formation, Nova Scotia

by

Ingrid Helmke

Submitted in partial fulfillment of the requirements for the degree of Bachelor of Science in Earth Sciences

at

Dalhousie University

Halifax, Nova Scotia

April 2024

Supervisor: Dr. Richard Cox

Table of Contents

List of Figures

List of Tables

Abstract

Along the North Shore of Nova Scotia, Canada vesicular basalts in the McArras Brook Formation are host to carbonate amygdules and veins. These basalts are interbedded within a well characterized Devonian strata but have not been directly dated. Through previous studies with U-Pb dating, the ages for calcite amygdules have been shown to form shortly after the eruption of the host basaltic lava. Secondary processes lead to the formation of overgrowths on existing calcite amygdules and low-T veins. These may form during tectonic emplacement and thus, multiple generations of calcite can also be found in the same suite of basaltic rocks. Before the U-Pb ages of both volcanism (amygdule formation) and later tectonic activity (secondary calcite) can be accurately measured and used as a proxy for the age of the basalt flows, the growth history of the calcite amygdules and viens must be carefully characterized. In this study we have used basic textural relationships and UV fluorescence to examine calcite growth history, both in the field and in collected samples. In-situ UV-fluorescence shows the growth of several generations of calcite amygdules and veins in the basalts from McArras Brook. We will use the UV characterization to help target analysis of different generations of calcite using a scanning electron microscope (SEM) to analyse the relationships between the fluorescence and the major elements. The results are expected to identify activator elements in the calcite which correspond to the differences in fluorescence colour, and correlate element compositions to the growth history. This will allow us to target the best areas for subsequent U-Pb dating of calcite to determine the absolute (volcanic) ages of these basalts, and the ages of secondary processes.

Keywords: Carbonates, amygdule, fluorescence, growth history, basalt

Acknowledgements

I.H. would like to acknowledge all the support in completing this study. Thank you very much to the lab technicians at Saint Mary's University, Mitchell Kerr in the Lapidary Lab, and Xiang Yang in the Electron Microscopy Centre. Richard Cox was a very helpful supervisor, providing the idea for this study. Huge thank you to Lydia Fairhurst for all of her help training me on all the equipment used, helping me analyze my results, and all of her other help every step of the way. Truly I could not have finished this thesis without her. Thank you to the Canadian Society of Economic Geology for the funding for this project.

1. Introduction

This study aims to characterize the carbonate amygdules in the basalt of the McArras Brook Formation, Nova Scotia, and determine their growth history. This study area is located on the North shore of mainland Nova Scotia, in McArras Brook. This study aims to answer the research question "what is the age and growth history of calcite amygdules in basalts of the McArras Brook formation, Nova Scotia?" This was completed using field in-situ analysis, including UV fluorescence; lab work including cutting samples into polished sections, analyzing the amygdules using X-ray mapping, back scattering electron (BSE) images, and energy dispersive spectroscopy.

Amygdules form shortly after the eruption of basalt, therefore these carbonate amygdules in the basalt formation are of interest because they can be correlated to the timing of eruption. Minerals used for dating igneous rocks typically include zircon, but there are no zircon in the McArras Brook basalt; therefore, the carbonate amygdules can be used for dating.

On the North Shore of Nova Scotia, exposed outcrop is seen along much of the coastline. This study is near Antigonish, Nova Scotia, near Arisaig (a local fossil-rich) Provincial Park. The McArras Brook Formation contains basaltic flows and red bedded sandstone units (Dostal et al., 1983). These basalt flows, and the amygdules they host are the interest of this study. The first McArras Brook basalt flow lies unconformably on a Silurian fossiliferous limestone unit (Dostal et al., 1983).

This basalt flow is abundant in amygdules. The amygdules are concentrated near the contact with the limestone, leading to the hypothesis that the abundance of calcite amygdules is due to the influence of this limestone during the eruption of the basalt. One hypothetical influence of the limestone would be calcite leaching from the limestone during the eruption, causing the abundance in carbonate amygdules.

Chapter 2: Geological Background

The geologic setting of the study area, and explore the nature of calcite growth, amygdule growth, and calcite fluorescence of the McArras Brook Formation will be discussed here.

2.1 Geology of Nova Scotia

The geological setting of this study provides key details for the results of this study. McArras Brook is in Antigonish County, Nova Scotia. The outcrops are exposed on the beach of the Northumberland Straight. The McArras Brook Formation is known to be Devonian in age based on the surrounding stratigraphy (Murphy, 2001),(Dostal et al., 1983).

The McArras Brook Formation lies disconformably on the Ardeness Formation, which is a marine, fossiliferous, oolitic limestone (Dostal et al., 1983). Within the surrounding stratigraphy, of interest is the underlying unit. The basalt formation of this study consists of multiple basaltic flows (Murphy, 2001). These rocks are part of the Merigomish Subbasin, which were deposited during episodes of regional orogenic activities in the Appalachian orogen, causing extension and basalt spreading centers (Murphy, 2001). During the Devonian, Nova Scotia experienced a pull-apart basin (the Maritimes Basin), causing these regional basaltic flows interbedded with sandstone (the McArras Brook Formation). This pull-apart basin opened the Merigomish Subbasin, what is now the Northumberland Strait (Murphy, 2001). These rocks were then altered during the Acadian Orogeny, causing the tilting of this sequence. The geology of Nova Scotia, and particularly the McArras Brook Formation and its relation to the Ardness Formation, provides the baseline geology for this study.

2.2 Carbonate Minerals in Amygdaloidal Basalt

Amygdule formation is critical to this study, and this section will outline their composition and characteristics. Amygdules are cavities, known as vesicles in igneous rocks, which are filled with secondary minerals (Rakovan, 2005). For this study, the igneous rock in question is a vesicular basalt. Amygdules do not appear in intrusive rocks, as the vesicles form from the dissolution of gases during eruption. In an intrusive rock there is no reaction with the surface to cause this dissolution, therefore amygdules only form in extrusive rocks. These vesicles are then filled with a secondary mineral. Though, calcite group minerals have end members that also react with HCl, and those will be discussed here as well. Calcite group minerals have a $CaCO_3$

structure, and cations can substitute into the structure for $CaCO_3$. Dolomite group minerals have a structure of $CaMgCO_3$.

Calcite is a carbonate mineral with a formula of $CaCO_3$. In this study we will also consider dolomite, which has a formula of $CaMg(CO_3)_2$, and ankerite which has a formula of $Ca(Mg,Fe^{+2},Mn)(CO_3)_2$. These different carbonate minerals can be stable under the same conditions, allowing for a locality to have a variety of carbonate minerals present (Bucher & Grapes, 2011, Deer, 1967).

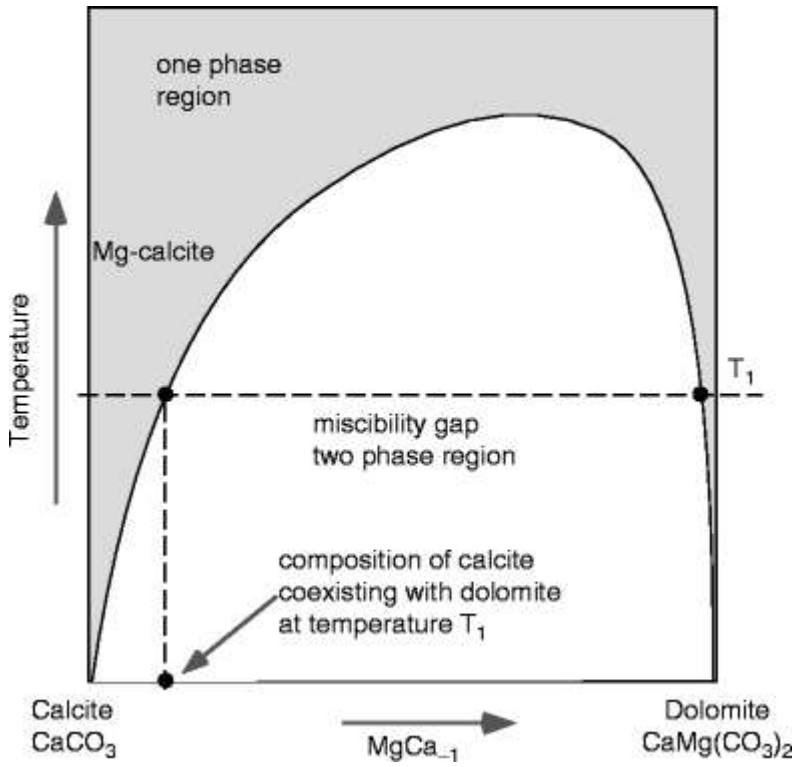

Figure 1. Diagram showing the temperature/composition of calcite and dolomite (Bucher & Grapes, 2011)

There are variations in the cell parameters due to substitutions into the crystal structure. The substitution of Mg for Ca causes an anisotropic contraction, and the substitution of Mn causes the interplanar spacings of calcite to be reduced by 3.3 %. (Deer 1967). $MnCO_3$ can exist and can form at relatively low temperatures, but this manganese-rich calcite will range from 0-50 mol%, as proven by Frondel and Bauer (1955). The substitution of Fe^{+2} is more common in dolomites and ankerite, than in calcite, though it is still possible (Deer 1967). The substitution of $MgCO_3$ into $CaCO_3$ is increased at higher temperatures. At 500°C the solubility is 5 mol%, but at 900°C the solubility is 27 mol%. With data from Goldsmith 1959, Deer produced graphically the

$CaCO_3$-$MgCO_3$ system, which demonstrates the transition from magnesian calcite to dolomite (figure 2) (Goldsmith & Graf, 1960).

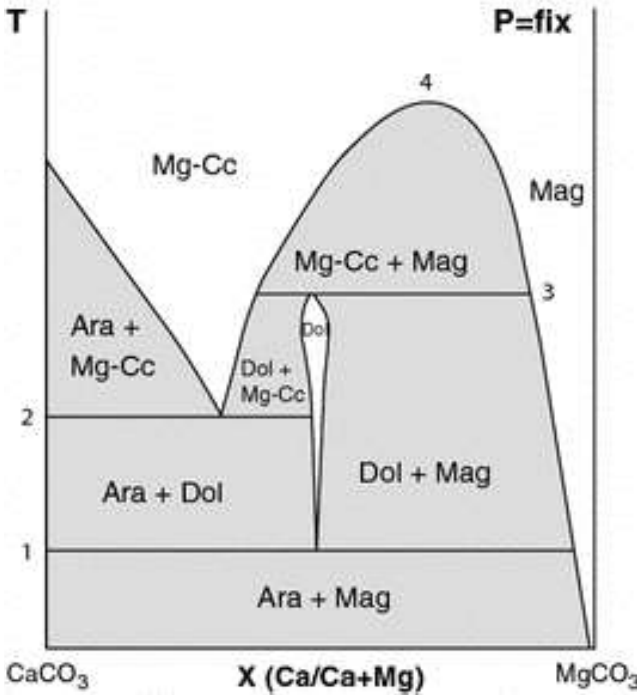

Figure 2. Stability of minerals in $CaCO_3$ and $MgCO_3$ composition. (Hermann et al., 2016)

Graff and Goldsmith (1955) point out the assemblage of dolomite and magnesian calcite in itself gives no information as to how much if any of the dolomite may have formed by exsolution and how much may have been in equilibrium with the magnesian calcite at elevated temperatures and CO_2 pressures (Goldsmith et al., 1955). This will have to be considered with the results of this study, as dolomite formed by exsolution would mean a lower formation temperature.

Calcite in the hard parts of marine organisms contained appreciable $MgCO_3$. (Chave, 1952) This is of interest because of the fossiliferous nature of the limestone unit of which the McArras Brook Formation overlies.

The process of calcite growth predominantly occur shortly after rock consolidation (within ~ 25 Myr) (Rembe et al., 2022). Therefore, dating the calcite phases in ocean floor volcanic rocks has the potential to constrain the timing of rock formation (Rembe et al., 2022), in both the crystallization of the basalt flow and the secondary deformation. The growth of calcite

in amygdules is key to understanding the age of the basalt, as the amygdules can be used as an age constraint of the basalt (within 25 Myr).

2.3 Calcite Fluorescence

Fluorescence in calcite is caused by a combination of trace element activators and quenchers. These each cause a reaction to ultraviolet light, causing the calcite to fluoresce. Fluorescence is caused by the excitation of electrons by ultraviolet light, that causes the release of energy in the from of a photon, which is light. Activators are the elements that undergo the change in electron balance. Sensitizers absorb some of the energy and transmit it to the activators, increasing the excitation energy. Sensitizers can have their own weaker emissions peak, but they will also increase the luminescence of the activator (Machel 1985). Quenchers suppress the activators and sensitizers, causing the luminescence to decrease. Quenchers can cause the peak of the wavelength of the activator to shift to a higher wavelength. They absorb excitation energy and undergo energy change without releasing photons. Machen 1985 organized a table of activators, suppressors, and quenchers in calcite and dolomite (Table 1).

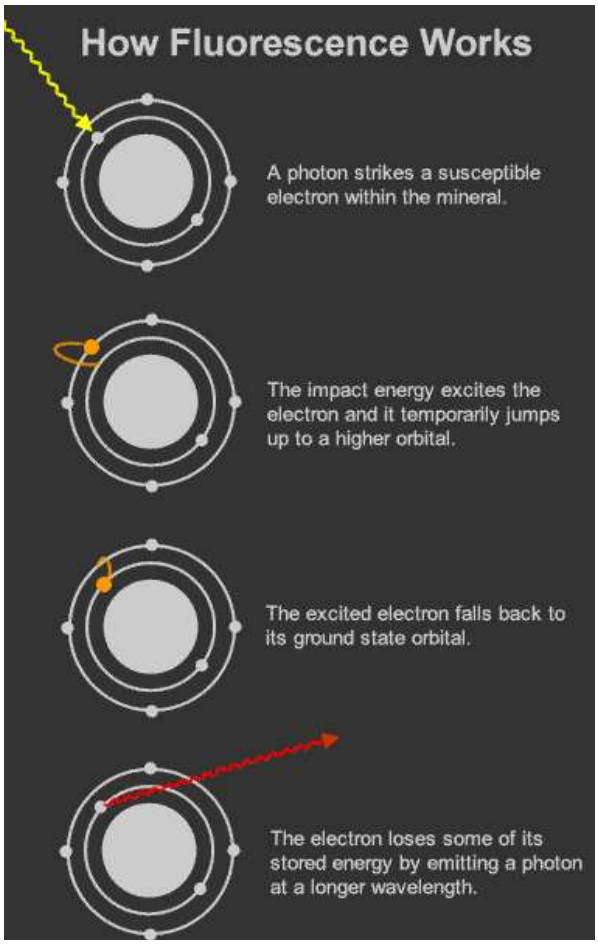

Figure 3. Diagram of how fluorescence works. (King, H. M.)

The colour of the perceived fluorescent light comes from the peak of the wavelength of the photon emitted. There can be multiple peaks excited at once, and these peaks can be perceived as one singular peak but may be multiple fluorescing together. Therefore, it is difficult to determine which activator or suppressor element is causing fluorescence, as it may be more than one (Machel 1985).

Brown (1934) demonstrated that the fluorescence of calcite is influenced by Mn, with it causing a red fluorescence. Mn causes a specific wavelength of 590nm in the fluorescence of calcite. The intensity of the

fluorescence of calcite increases with increasing Mn, up to a maximum of 3.5% $MnCO_3$ (Brown 1934).

Table 1. Activators, Sensitizers, and Quenchers for fluorescence in calcite and dolomite (Machen, 1985).

Activators	Sensitizers	Quenchers
Mn^{2+}	Pb^{2+}	Fe^{+2}
Pb^{2+}	REE	
REE		

Chapter 3: Methods

3.1 Study Area and Sample Collection

For this study, a total of nine samples were taken from five areas of interest. This collection was on McArras Brook beach in Arisaig, Nova Scotia, accessed via John Jones Ln. Before samples were gathered, a controlled sketch was done of the main study area, locality 28-08-23-1. Once the area was sketched and characterized, the outcrop was evaluated for which samples to collect. For this we chose four collection sites at the first outcrop. In-site UV fluorescence was complete on the sample area, giving us a view into the growth history via the UV fluorescence before analyzation in the lab. A 4lbs sledgehammer was used to detach the samples from the basalt unit. Each sample was then labeled and stored in a sample bag and returned to the lab.

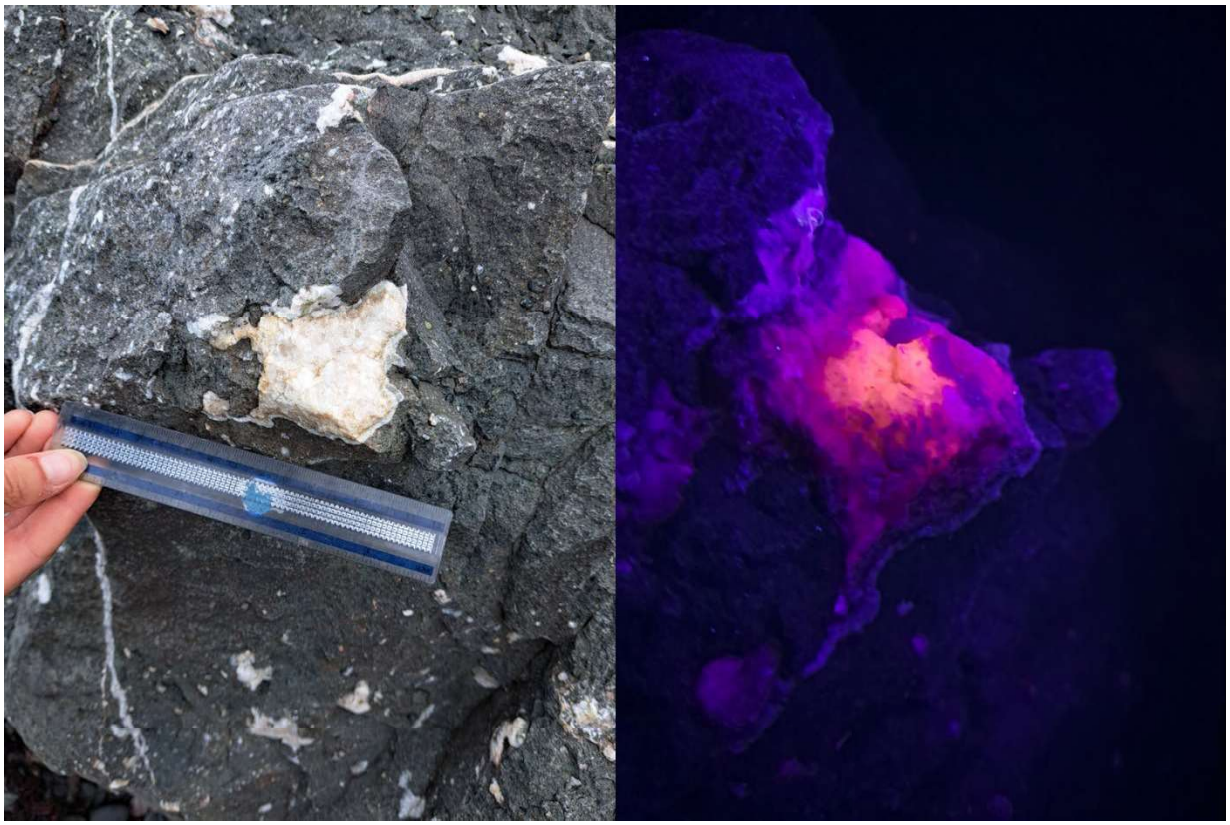

Figure 4. Comparison of calcite amygdule in the McArras Brook basalt, field shot in daylight and under UV.

Figure 5. Field photos of calcite veins in the McArras Brook basalt, in incident light and UV.

3.2 Sample Preparation and Second UV Characterization

When returned to the lab, the samples were labelled and sorted. The samples were then cut into slabs ranging from 0.5 inches to 1 inch. These were cut with a friction saw. This was done to expose a fresh surface of the basalt and the amygdules. The slabs were then cleaned with water to ensure a clear surface. The slabs were imaged in incident light and under UV, with labels and a scale card for reference. The UV light was a short wave (254nm) Mineralight lamp (model UVGL-55). The colours seen under UV fluorescence range from red to pink to purple. These are indicative of different activator elements within the calcite structure. For example, the red fluorescence represents an activator element of Mn (Machel, 1985). Initial conclusions seen under UV include changes to calcite composition from generations of growth and basaltic flows, respectively.

After initial analysis from UV characterization, the cut slabs were further cut using a low-speed saw into 2mm-5mm thick slabs, with an area of 2.5cm^2. The samples were then transferred

to Saint Mary's University and cut there. There, the laboratory technicians were able to cut the samples into 0.5-1.5cm pieces.

The sample pieces were then mounted in 2-3cm round moulds, and had resin added. The epoxy rounds were then grinded using 180–420-micron grit grinding paper. The grinded rounds were then polished using 1 micron and 0.3-micron alumina powder on a polishing wheel.

Polished samples were then imaged under incident light using a binocular microscope. The samples were imaged using an AmScope microscope digital camera, (model MD500L), and an AmScope LED-56S LED ring light set up to illuminate the sample, under a Leica MS-5 microscope on 1.6x and 0.63 magnification.

Polished rounds were then transferred to Saint Mary's University for X-ray mapping. X-ray mapping was completed using a scanning electron microscope (SEM). At Saint Mary's University the SEM was operated within the Electron Microscopy Centre. For the processing of the data, we used the program Aztec to create the X-ray maps and data collection. The SEM used was Oxford Instruments X-Max 80mm^2 Tescan mira 3, which is a field emission SEM. We used a beam intensity of 10-12, with a 7-10nm beam size. Point element data, and average area data was collected, X-ray maps were made of the samples from the center of the crystal to the rim.

We performed point analyses for specific inclusion in the calcite amygdules. For generic calcite amygdule information, we used area average counting, which provided data of major elements from an area, which allowed for more statistically significant data collection. The major elements we measured were Ca, Fe, Mg, Mn, and Al. Oxygen and Carbon-coating were ignored, as they are abundant in calcite, and not of interest for this study. Then BSE maps were calculated, focusing on the same major elements. Maps were made on sample 28-08-23 1a, 28-08-23 1b, and 28-08-23 1d.

Then the data was restricted to carbonate minerals only (Ca, Mg, Mn, Fe) and was calculated to be normalized to the percentage with respect to the total cation. Then this value was inserted into the carbonate calculation table (from gabbrosoft.com) which yields the formula number of Mg. This value was then inserted into the Mg-in-Calcite excel sheet which yields a temperature of the formation of calcite. This calculation is only valid with calcite with Mg, therefore minerals with high Mg such as dolomite were not able to be calculated. These

temperature results will be discussed below. The data collected from the SEM was used to make Ca-Mg-Fe ternary plots for each sample. This demonstrates which proportions of the samples are calcite and which are dolomite or ankerite.

Aluminum presented itself to be a problem, as alumina grit was used in the polishing of the sample, therefore if there were any pits in the sample, the aluminum concentration may be much higher than naturally occurring. Aluminum was excluded from cation calculation for this reason.

Chapter 4: Results

Using the data collected from field work, lab work, and scientific analysis we found temperatures of the formation of the calcite amygdules, along with the composition of some of the inclusions in the amygdules. The SEM data and BSE images allow a comparison between the composition of the calcite, the incident light view, and the fluorescence.

Sample 1a

Figure 6. Sample 28-08-23 1a in incident light, under the microscope.

Sample 28-08-23 1a in incident light shows that it is not a uniform carbonate growth. There are areas with different colours, some pale orange/pink, some opaque/white, and some green (Figure 6). There are also bright white areas, which in the X-ray maps appear to be silica rich (Figure 7). There are also fractures seen in the sample, which so not align with any cleavage planes.

There were X-ray maps taken at multiple localities within the amygdule. Locality 1 is shown in Figure 7, and locality 2 is shown in Figure 8. In these X-ray maps we can see the

relationships between the different elements within the amygdule, and relative abundance. In Figure 7, we see that there are silica rich areas (pink), which appear as white in plane light. It appears here that there is a lower boundary of Mn, but there is no clear replacement. We see it is still calcite as there is an even amount of Ca throughout this boundary. The silica rich and magnesium rich areas are irregular, not a regular growth pattern. Indicating both dolomite and quartz may have formed from exsolution. When comparing to the incident light images, to X-ray the dolomite appears to correspond to the green areas in incident light (Figure 6 and 7).

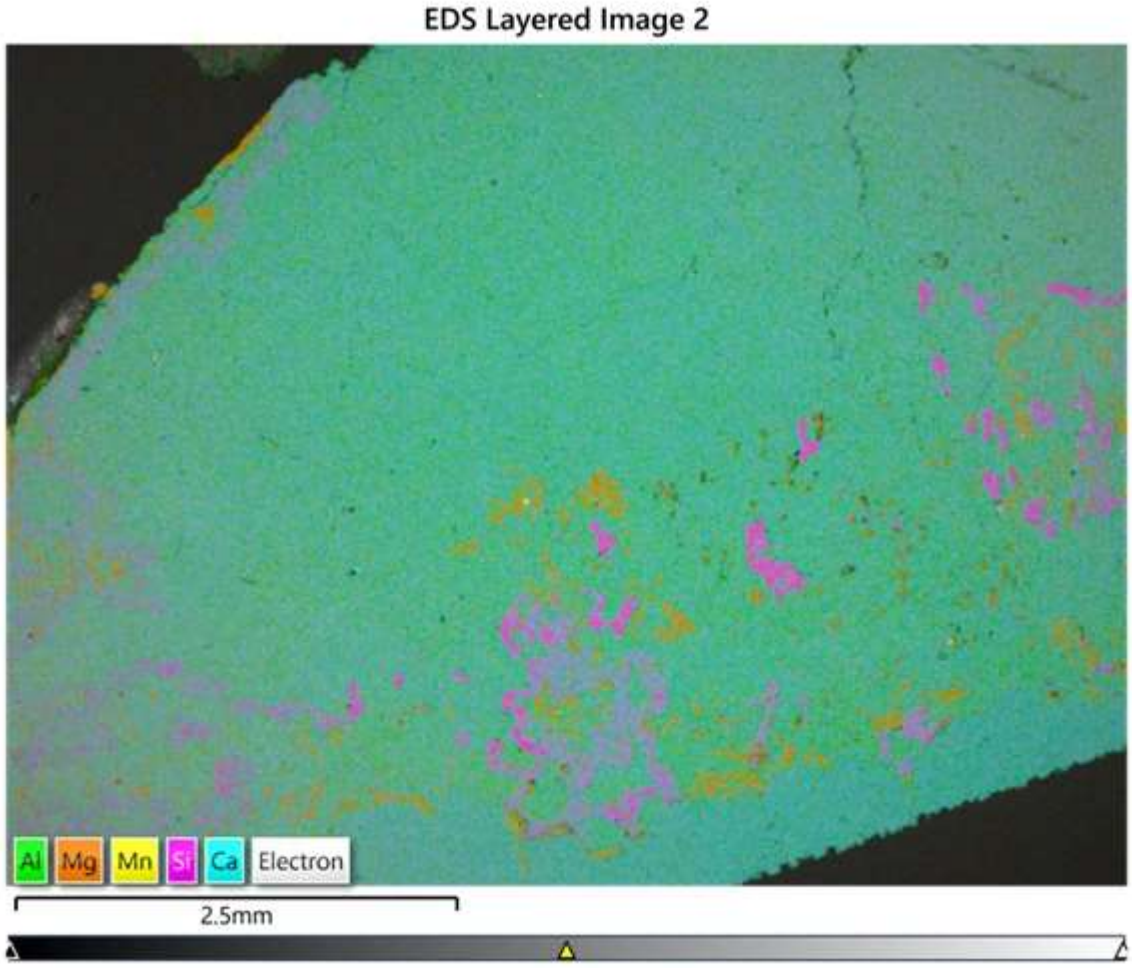

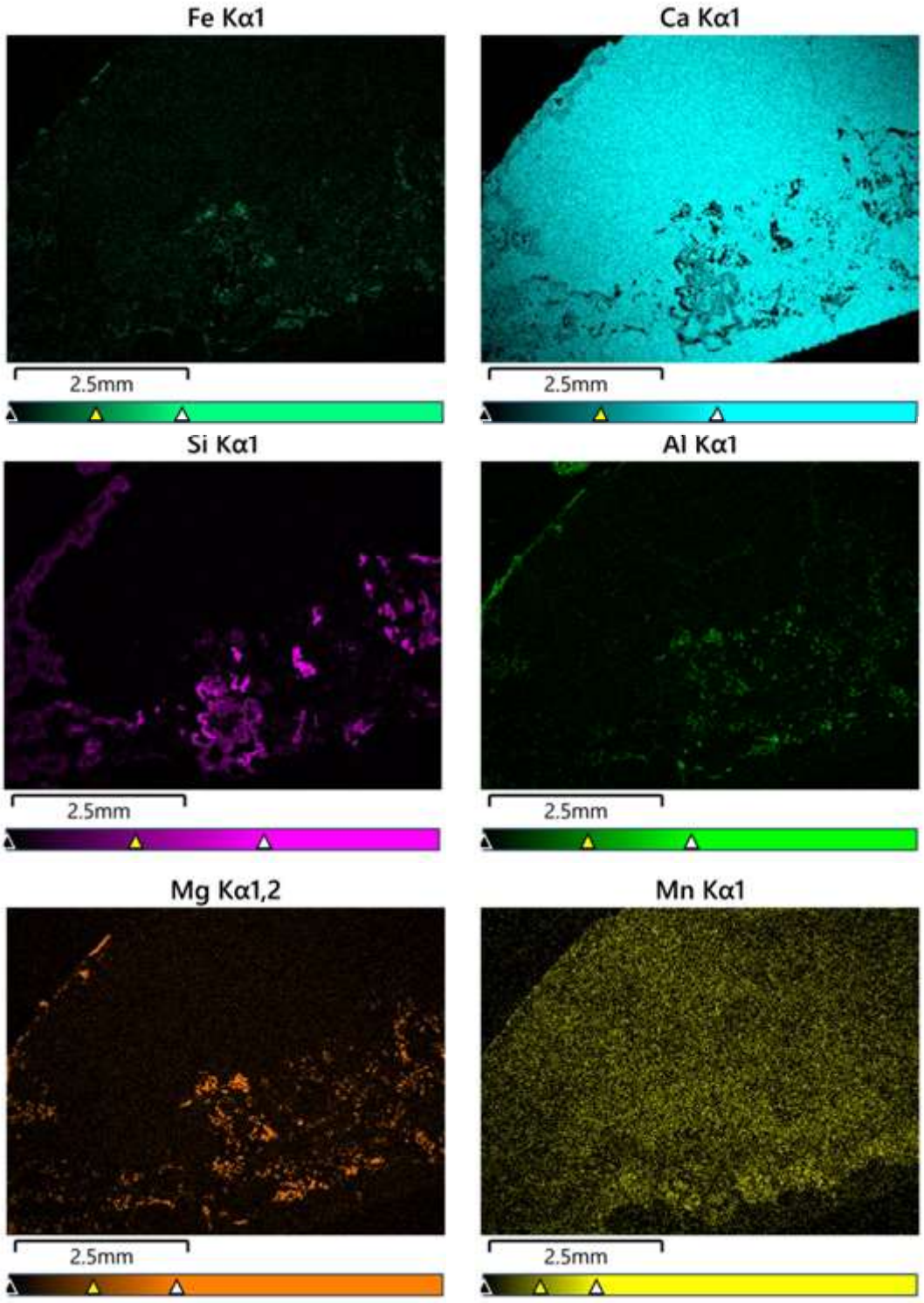

Figure 7. X-Ray maps of sample 28-08-23 1a, locality 1.

In locality 2 of 28-08-23 1a, we see a silica rich rim, with a calcium rich core. Manganese is present throughout, but less abundant within the rim and core then outside of it (Figure 8).

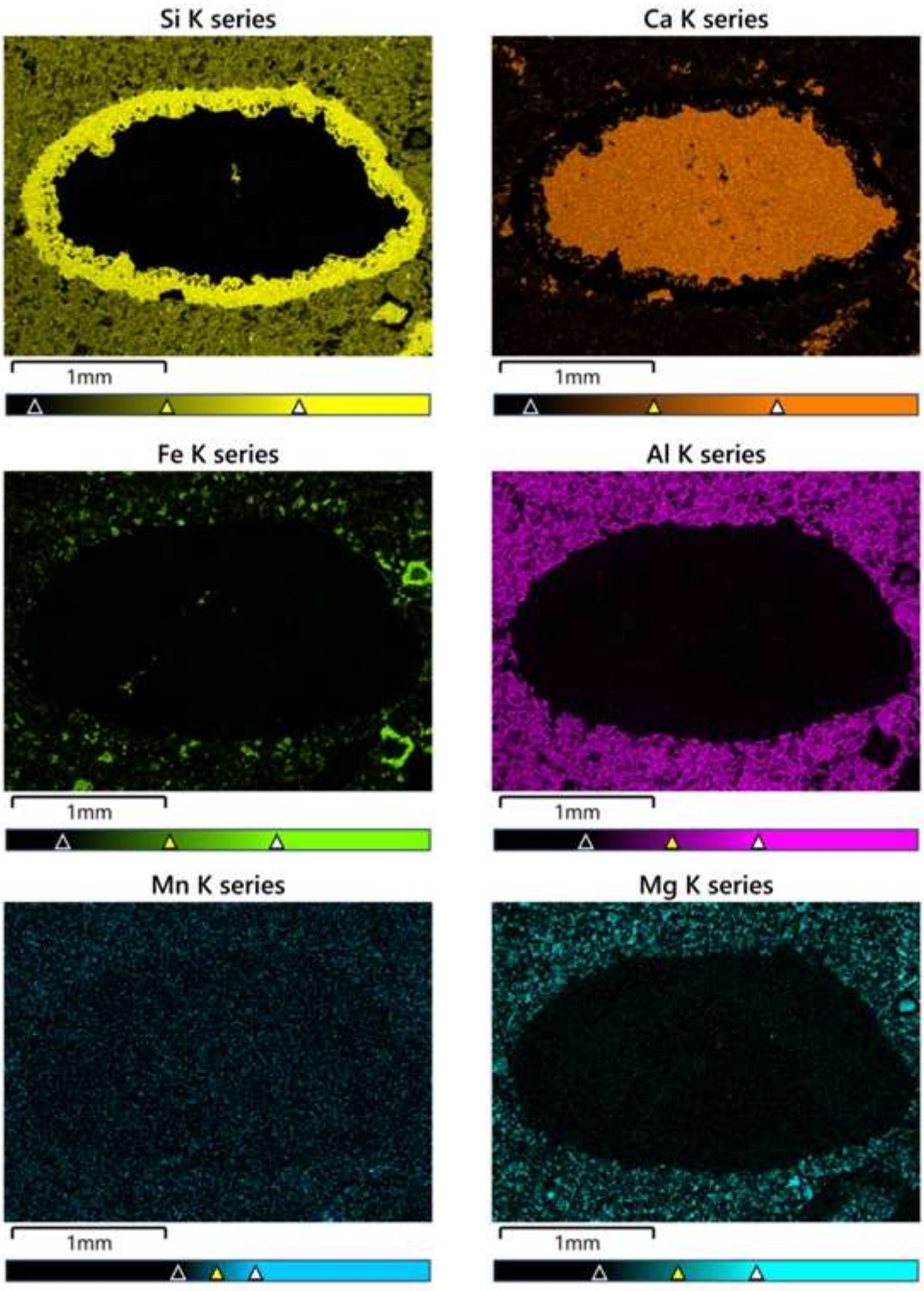

Figure 8. X-Ray maps of sample 28-08-23 1a, locality 2. Taken with the SEM at Saint Mary's University.

Then there were 4 BSE images taken, we can see the locations of the compositional data taken, which is presented in appendix 1, and we can see areas of changes in heavy rare earth

elements (HREE) as lighter or darker areas. Brighter white in the BSE images indicates a higher abundance of HREE (Figure 9).

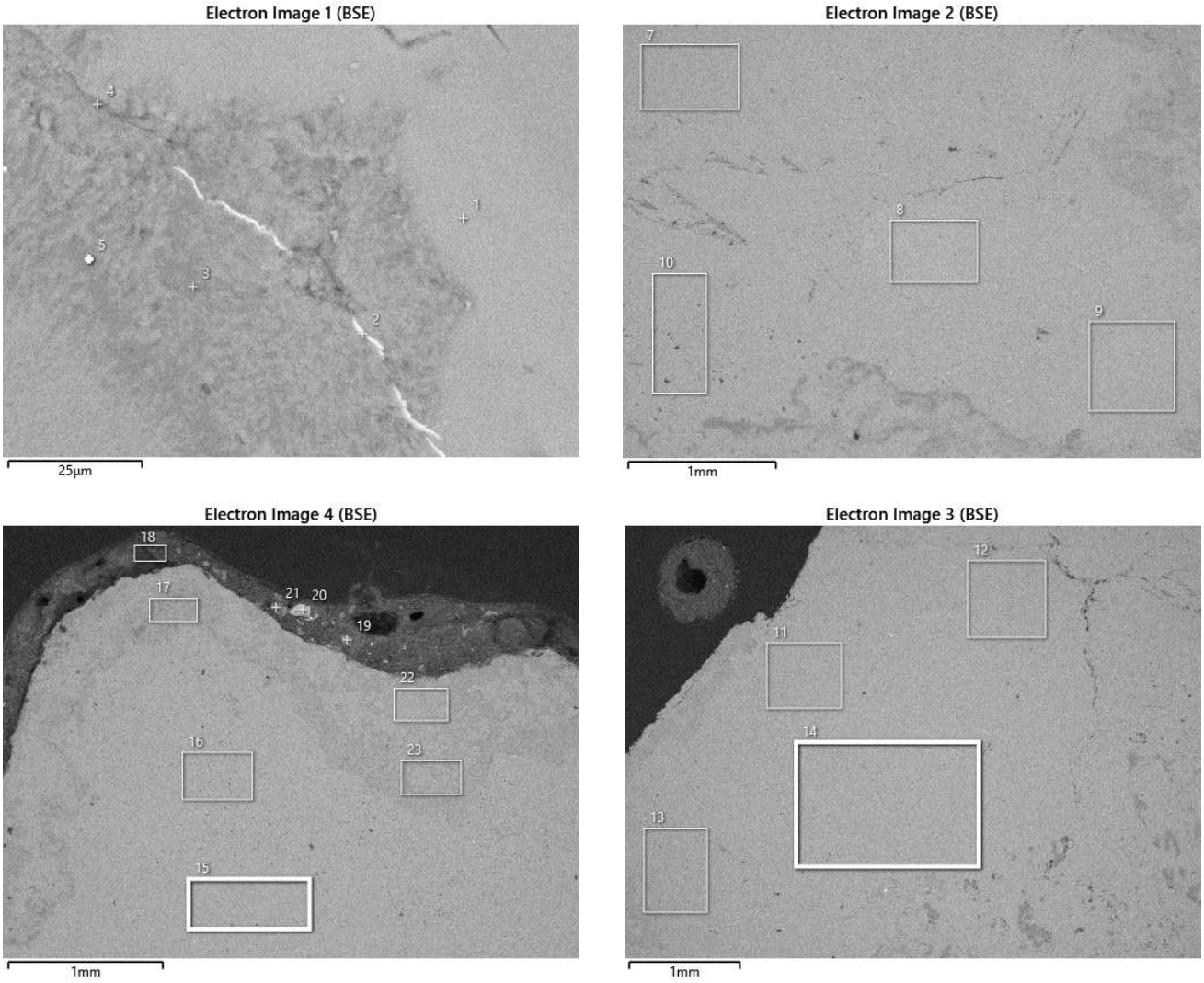

Figure 9. BSE images for sample 28-08-23 1a.

Using this EDS data (Appendix 1) estimated temperatures for the amygdule formation was calculated. These results are presented in a later section, showing the temperatures from valid points. Some points did not yield a reasonable estimated temperature because of element abundance.

Sample 1b

In sample 28-08-23 1b incident light images were taken showing the carbonate amygdule (Figure 10).

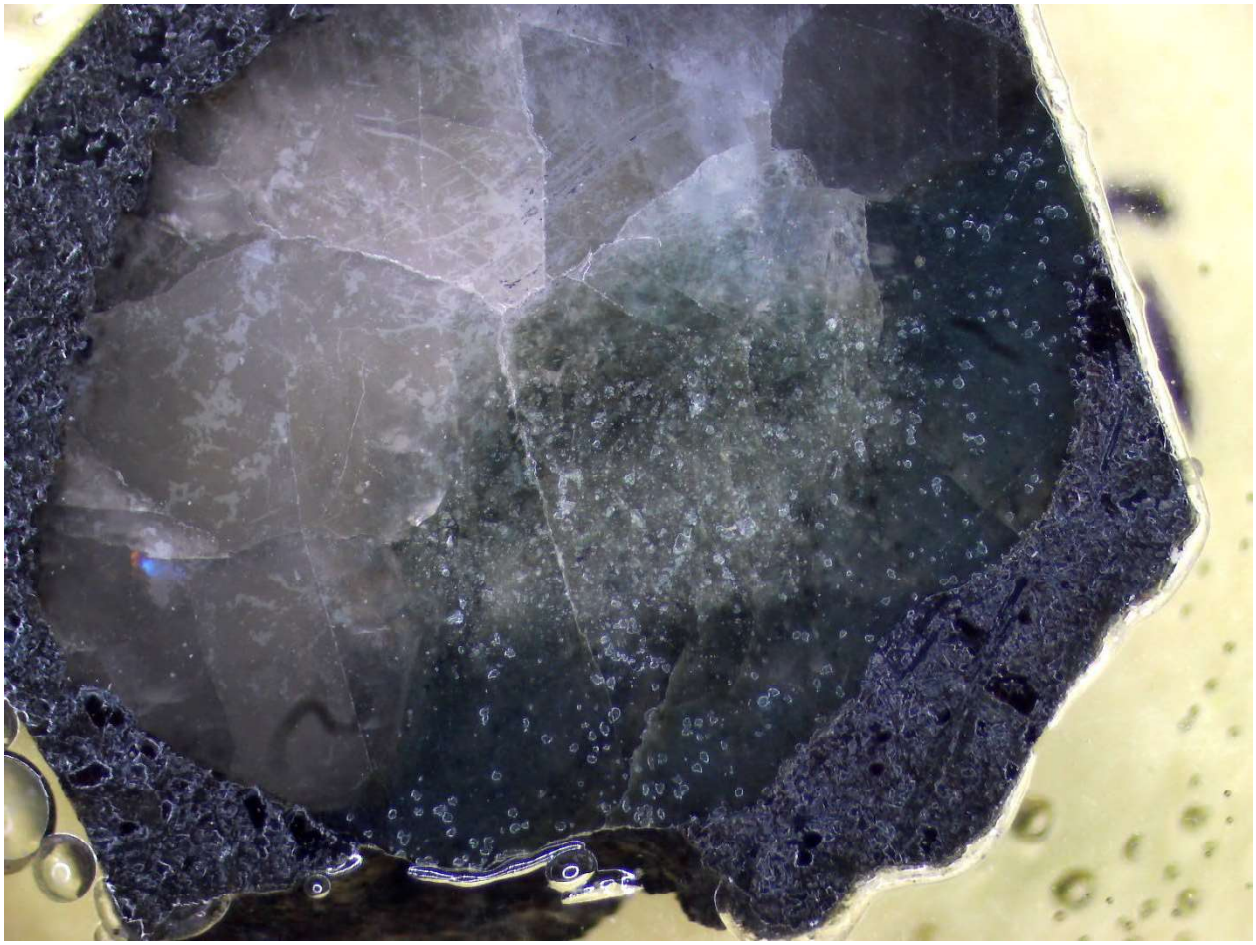

Figure 10. Incident light image of sample 28-08-23 1b.

We can see areas of different coloured carbonate; roughly half of the amygdule is clear or white, and the other half is cloudy green. There are fractures within the carbonate amygdule, which appear as though they could be boundaries for different colours of the carbonate.

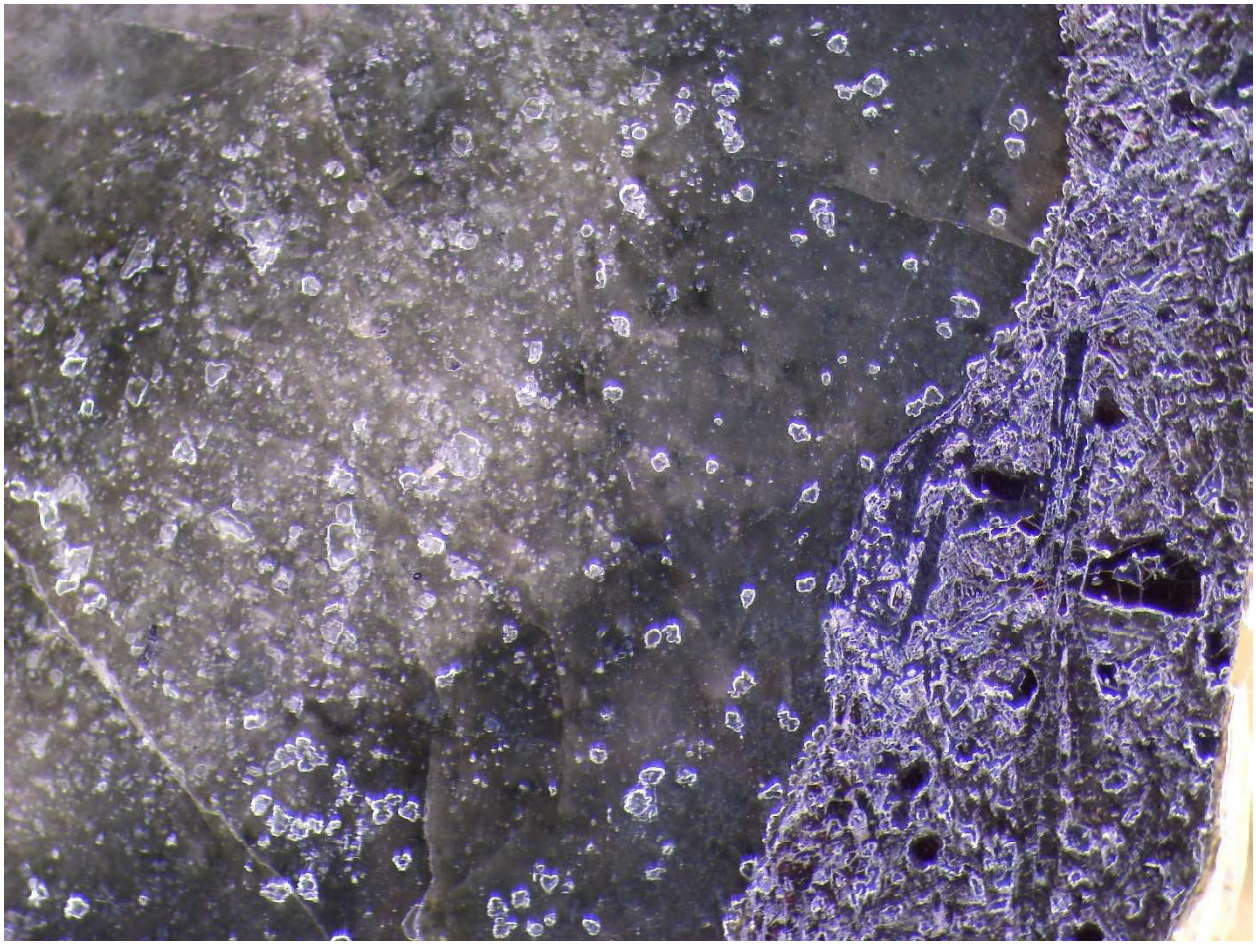

Figure 11. Incident light image of sample 28-08-23 1b, focused on the grain boundary on the green half of the amygdule.

The bright white areas within the amygdule match the characteristics of the basalt (on the right of Figure 11). The amygdule is not a consistent colour, it is irregular. There could be some zoning present, with the area of grey-green at the rim, which could be concurrent with the Mn abundance in figure 14.

We can see fractures in the amygdule that does not appear to be aligned with any cleavage plane (Figure 12).

Figure 12. 28-08-23 1b, incident light image of the amygdule, focused on the cloudy white side of the amygdule, showing also the grain boundary and the contact with the green side of the amygdule.

The green half of the amygdule contains bright white areas, which in the X-ray maps appear to be silica rich (Figure 13). The green area of the amygdule is not a consistent colour throughout; it appears to be darker in areas, with a lighter and paler green center (Figure 13).

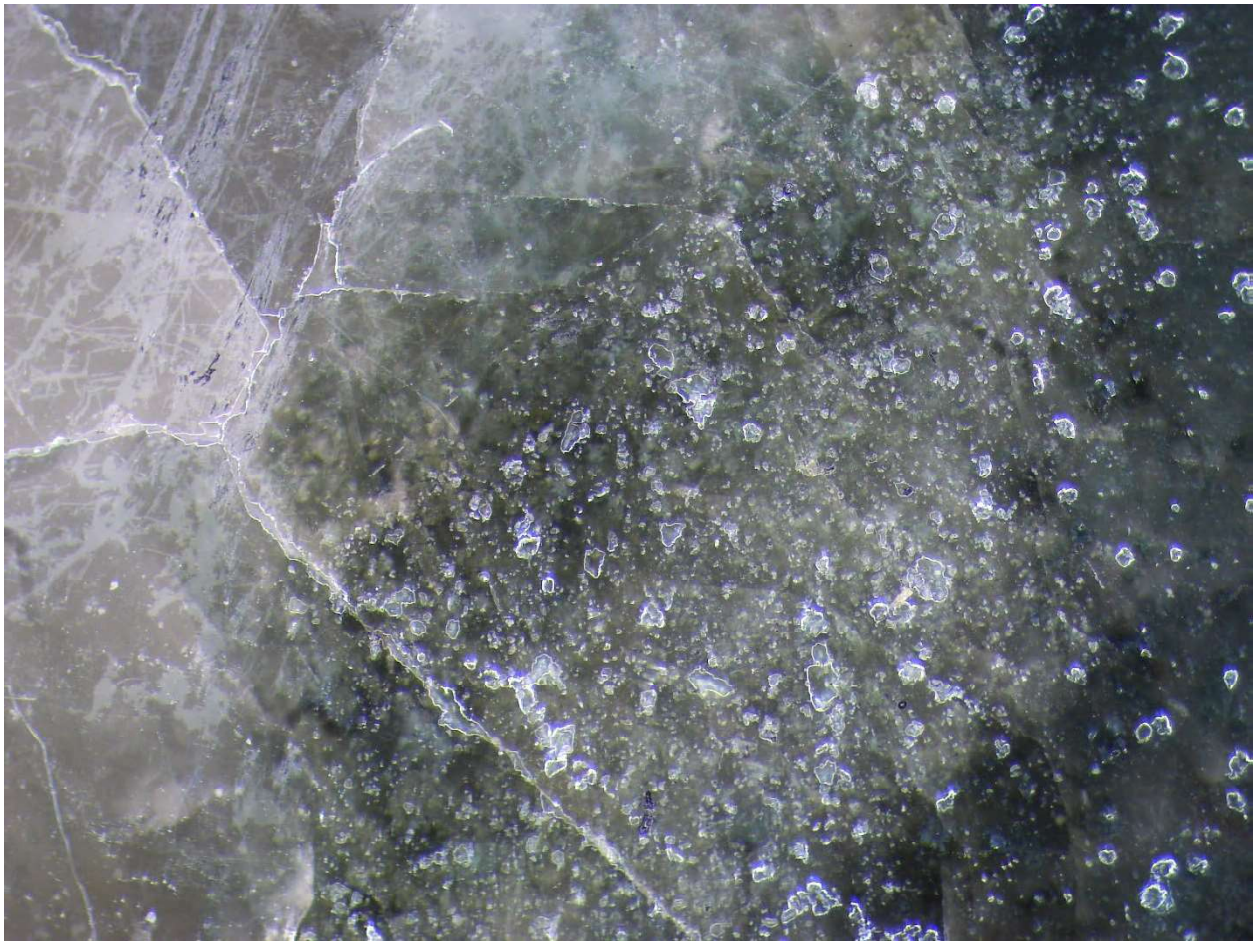

Figure 13. Sample 28-08-23 1b imaged in incident light, showing the contact of the white/clear half of the amygdule and the green part of the amygdule.

X-ray maps of sample 28-08-23 1b show the relative abundance of elements in the carbonate amygdule. There were two x-ray maps taken at two different localities within the amygdule (Figure 14 and Figure 15).

EDS Layered Image 1

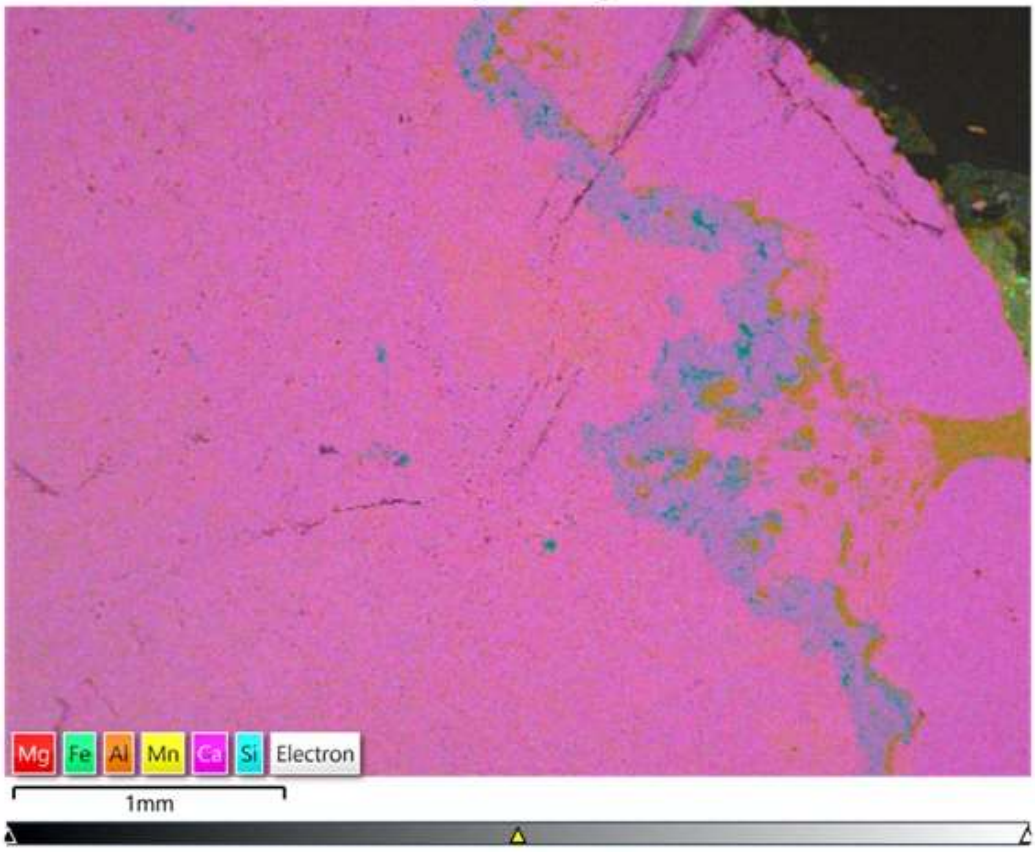

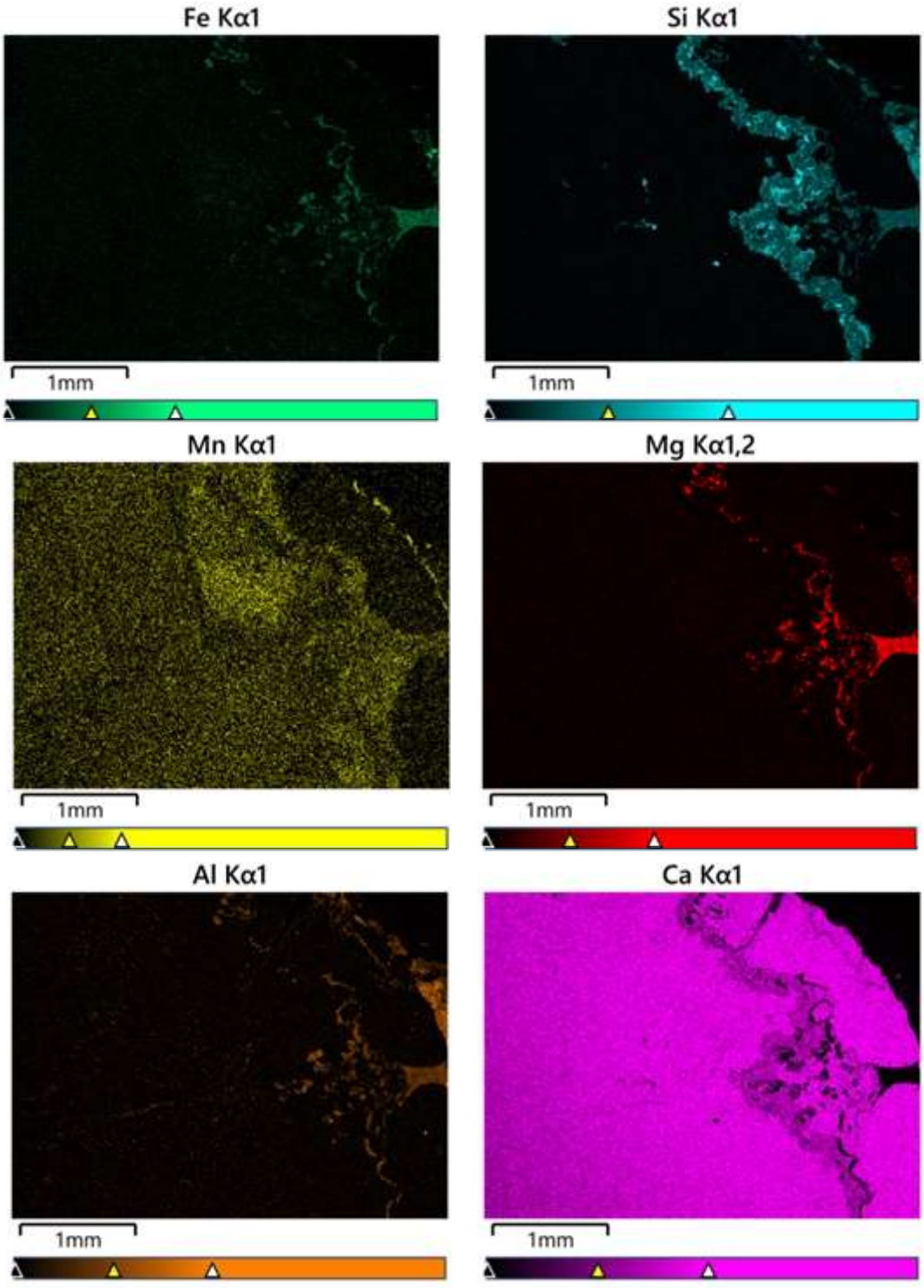

Figure 14. X-Ray maps of sample 28-08-23 1b, locality 1.

It appears there is a connection of the amygdule to the basalt host rock. This contact has no Ca, but very high Mg. We see an abundance of Si coordinating with lower Ca levels, so there may be

a thin layer/vein of quartz. In the Mn map, there is a concentration of Mn in the centre of the map, but no other clear replacement element.

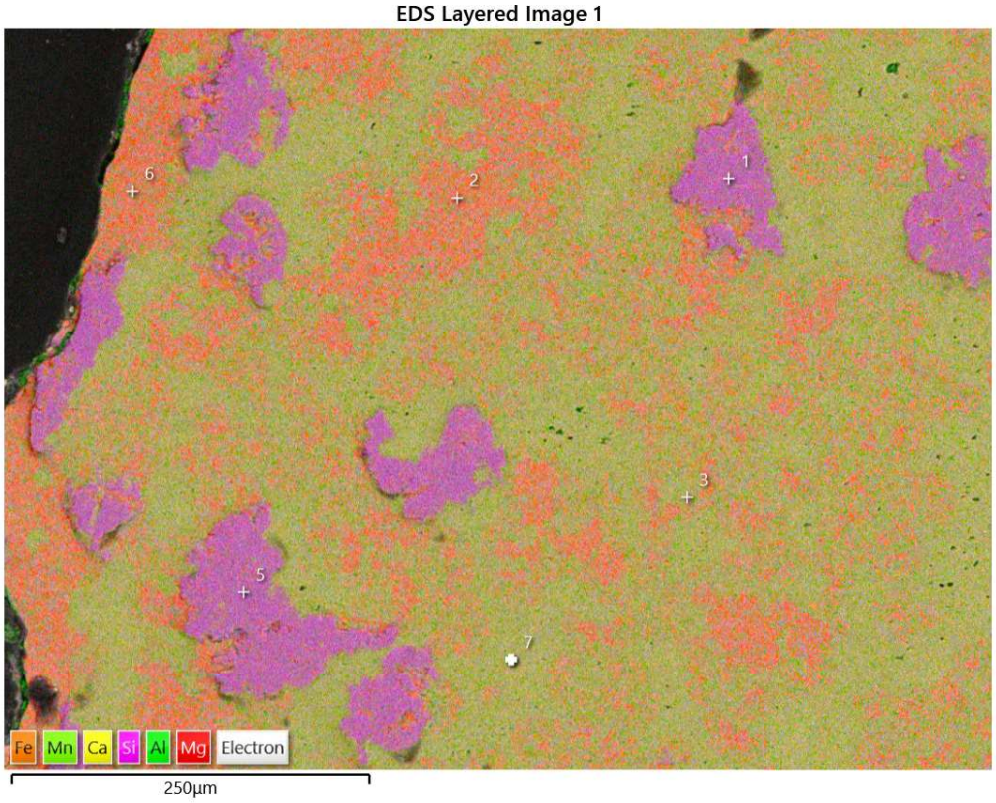

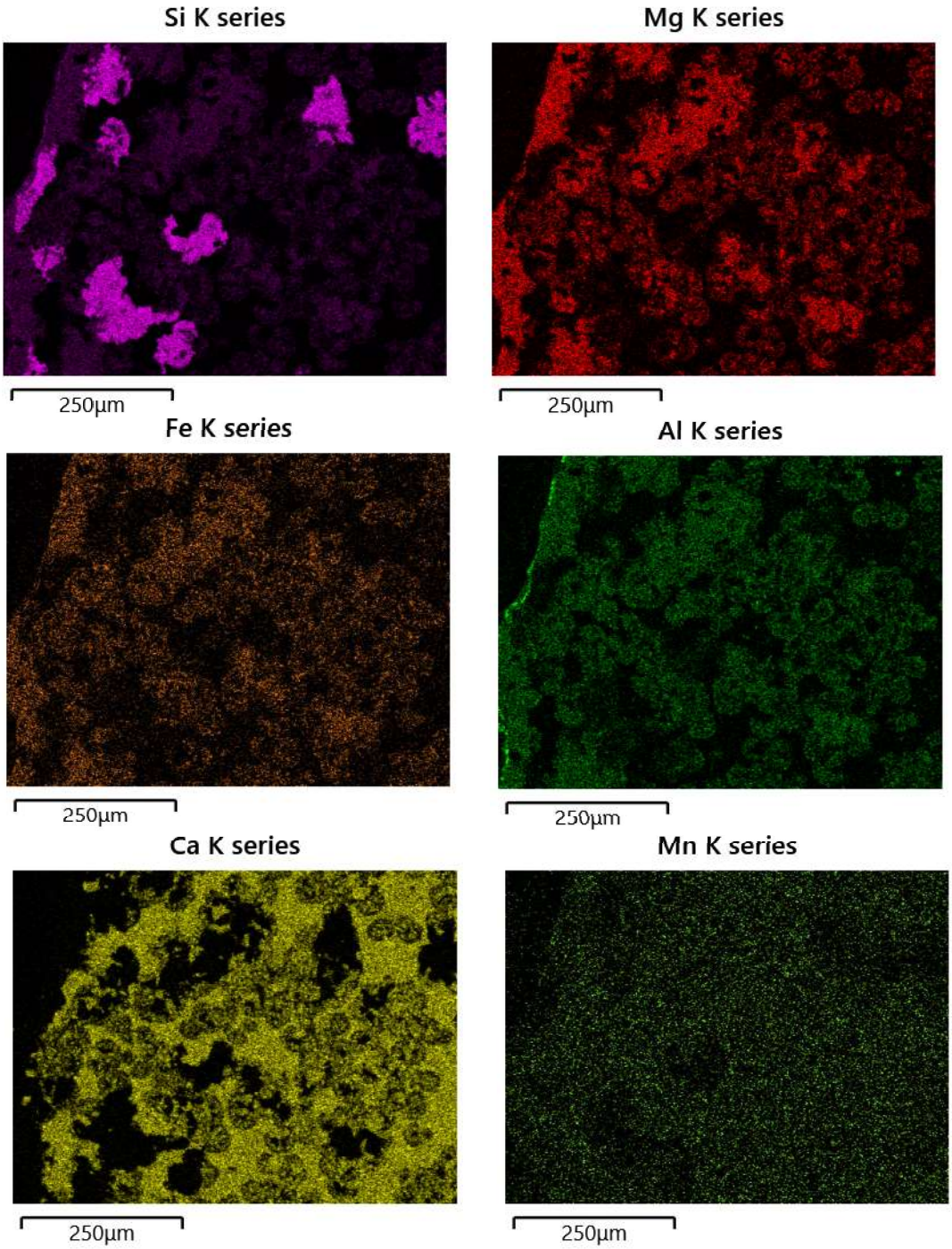

Figure 15. X-Ray maps of sample 28-08-23 1b, locality 2.

There is no clear correlation between the major cations in locality 2 (Figure 15). The silica rich zones correlate to the Ca depleted zone, but in the carbonate cations (Fe, Mg, Mn, Ca, Al) there is no correlation between their occurrences (Figure 15).

BSE images were taken on the SEM (Figure 16). There are two BSE images for sample 28-08-23 1b, which are both shown below. BSE image 1 in Figure 16 corresponds to the X-ray map in Figure 15.

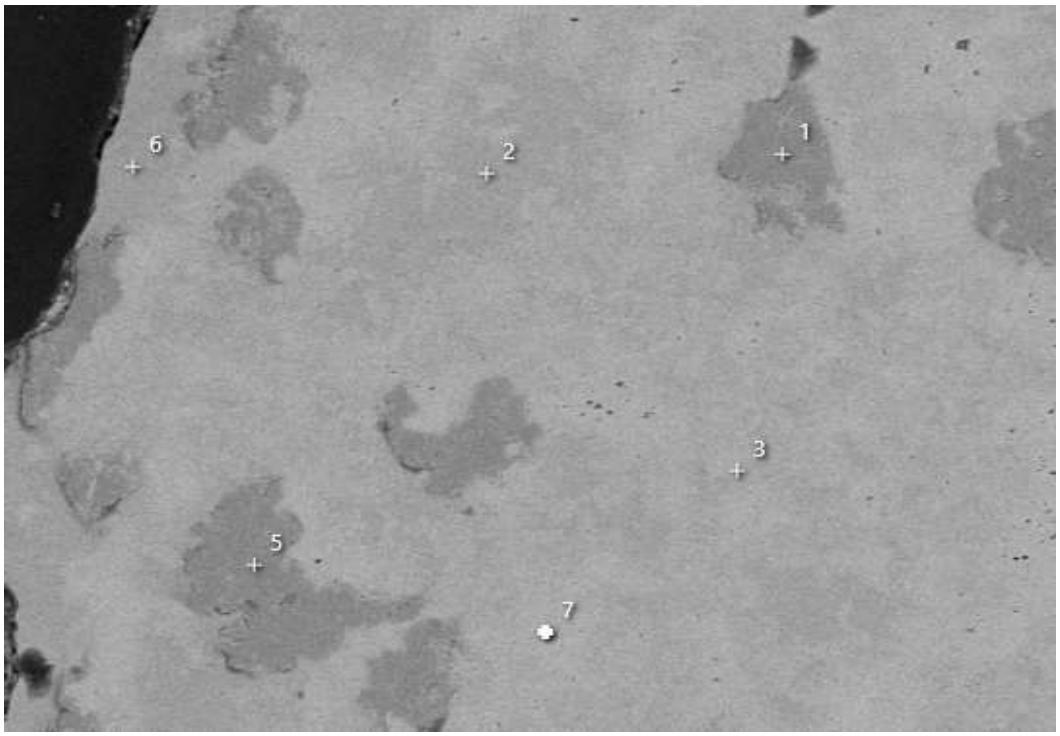

Electron Image 2 (BSE)

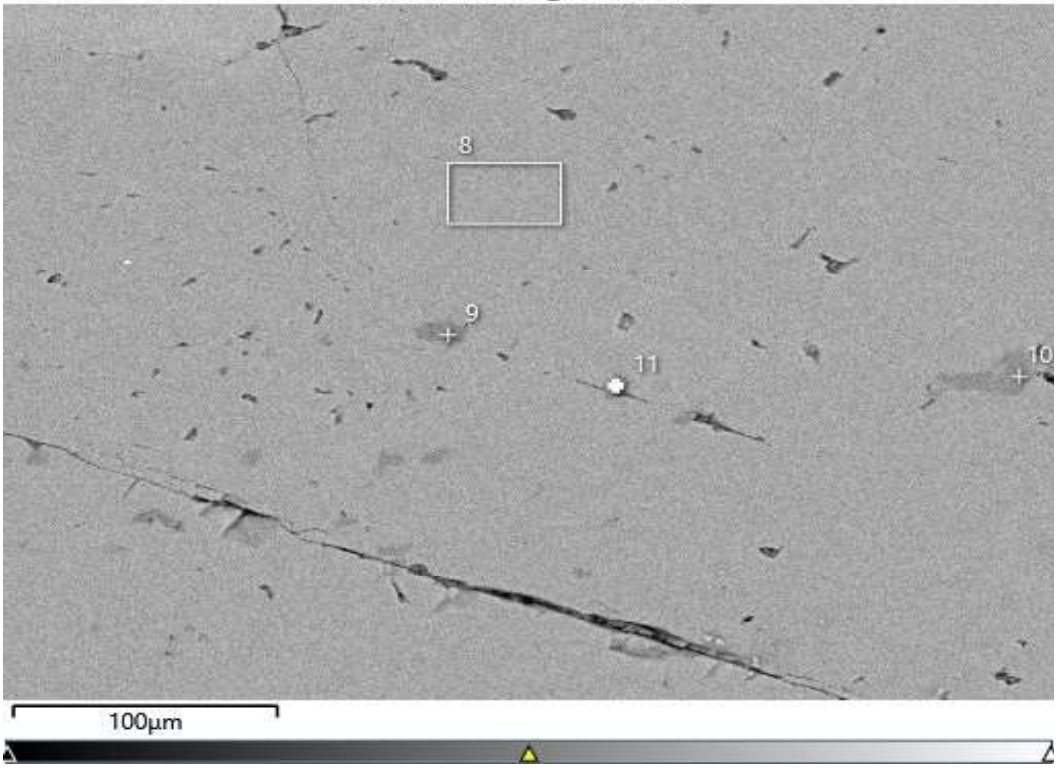

Figure 16. BSE images of sample 28-08-23 1b. Numbers shown indicate the location of the EDS data shown in appendix 1.

Sample 1b shows very inconsistent growth; the X-ray maps are splotchy, and show irregular growth patterns. The incident light images show that the amygdule is not clearly zoned, or a consistent colour.

Sample 1d

Sample 28-08-23 1d was imaged in incident light. The carbonate amygdule is zoned, showing a darker rim, and a cloudy white interior (Figure 17). The core of the amygdule has a pit, and within the pit we can see euhedral crystals. There is a fracture that extends throughout the entirety of the amygdule, through the pit.

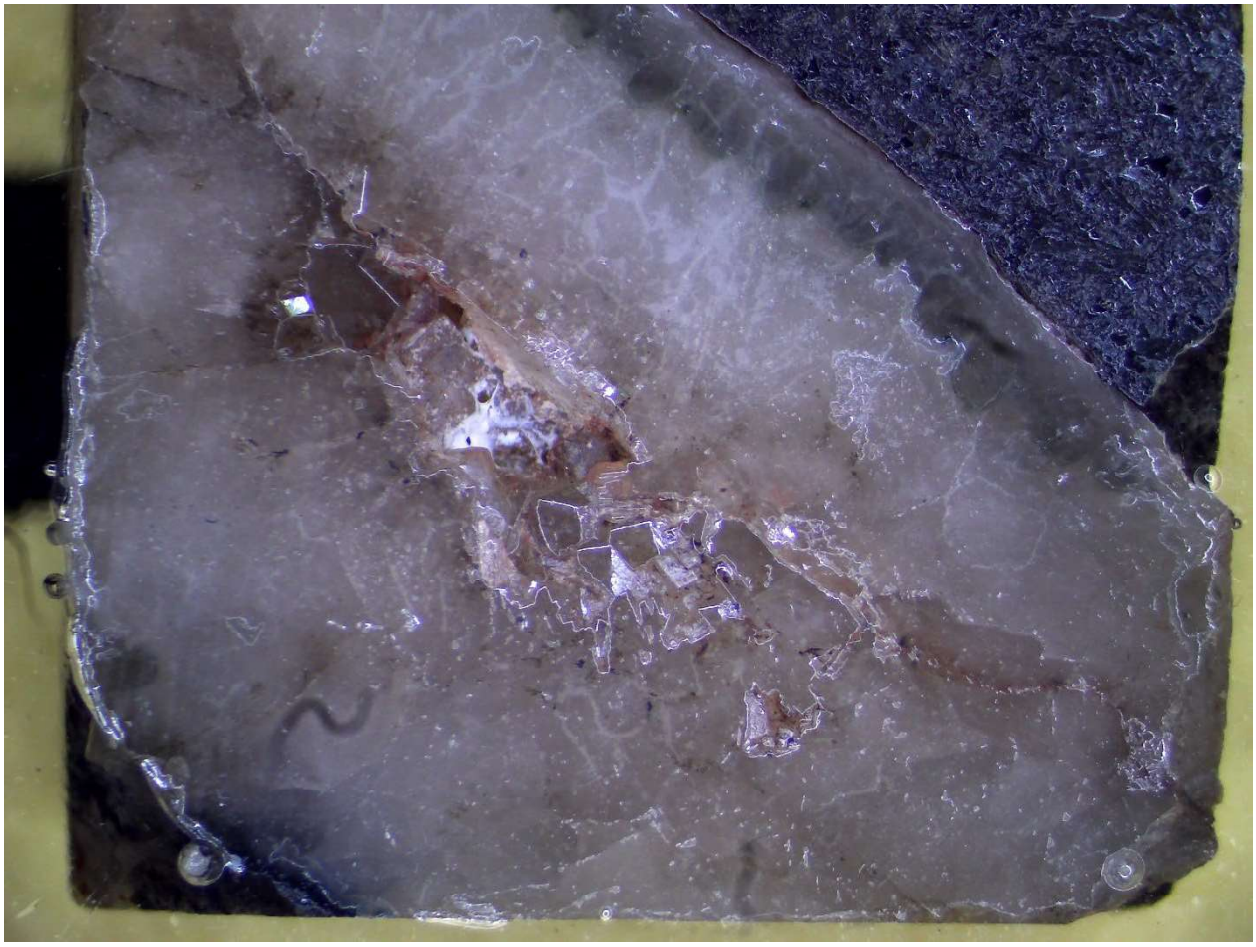

Figure 17. Incident light image of sample 28-08-23 1d.

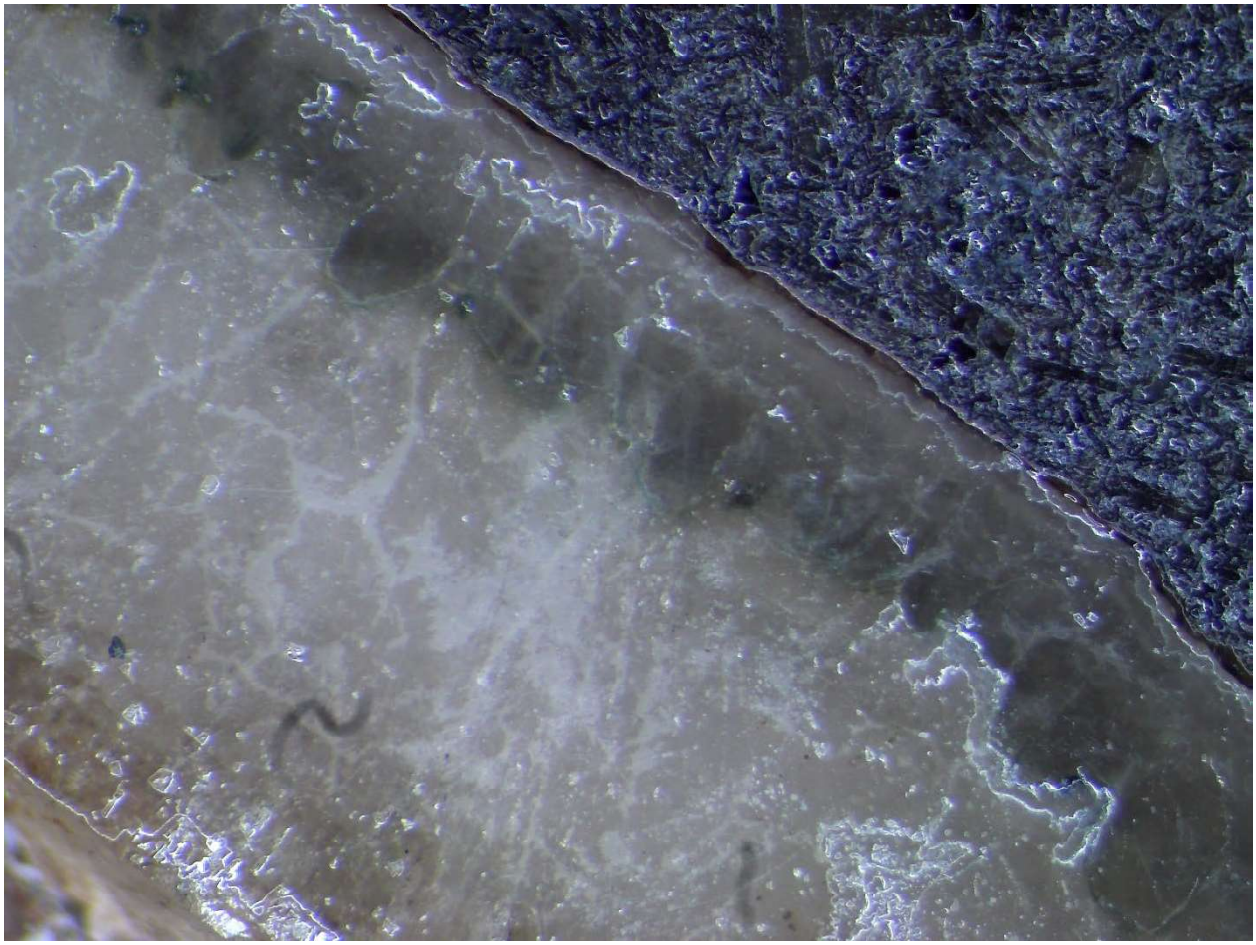

Figure 18. Incident light image of sample 28-08-23 1d of the study area of x-ray maps.

The contact with the basalt and the amygdule has a green rim, and an uneven boundary with the cloudy white/grey. There are bright white areas that appear silica rich in the SEM images (Figure 20).

The BSE images in Figure 19 show the locations of the EDS data that was collected (Appendix 1). BSE electron image 1 shows the pit in the centre of the amygdule, and the euhedral crystals.

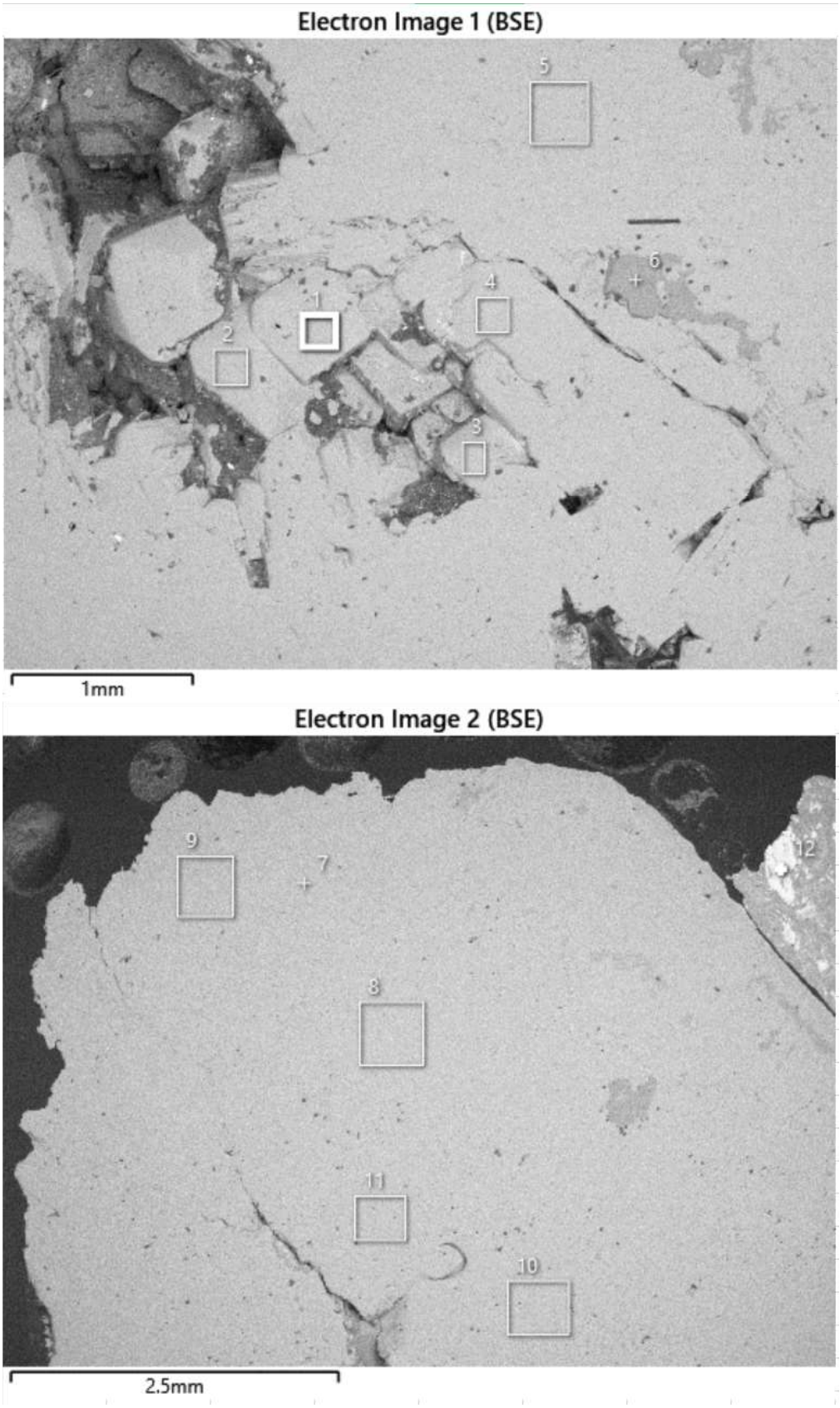

Figure 19. BSE images of sample 28-08-23 1d.

X-ray maps of sample 1d how the major cations that are present in this sample, and is from the same position as Figure 18.

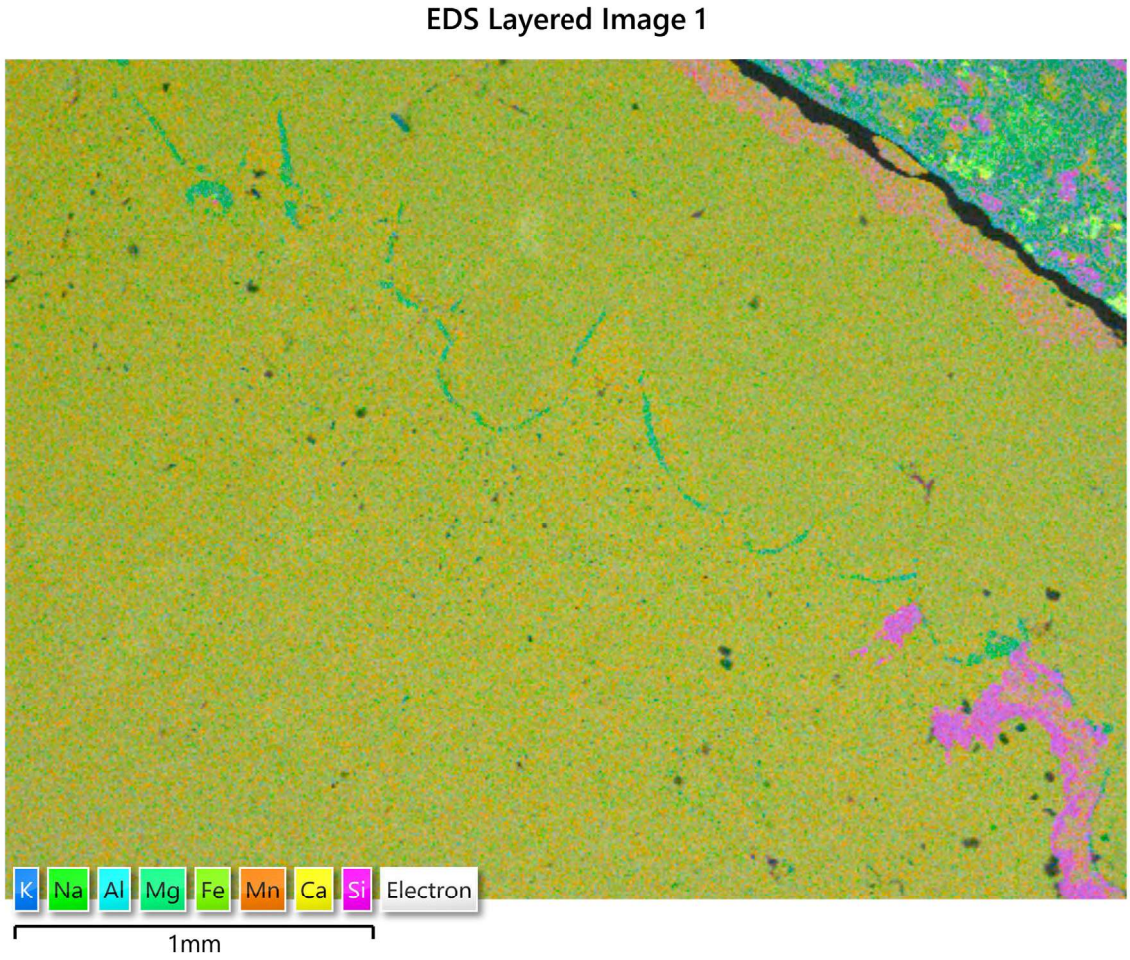

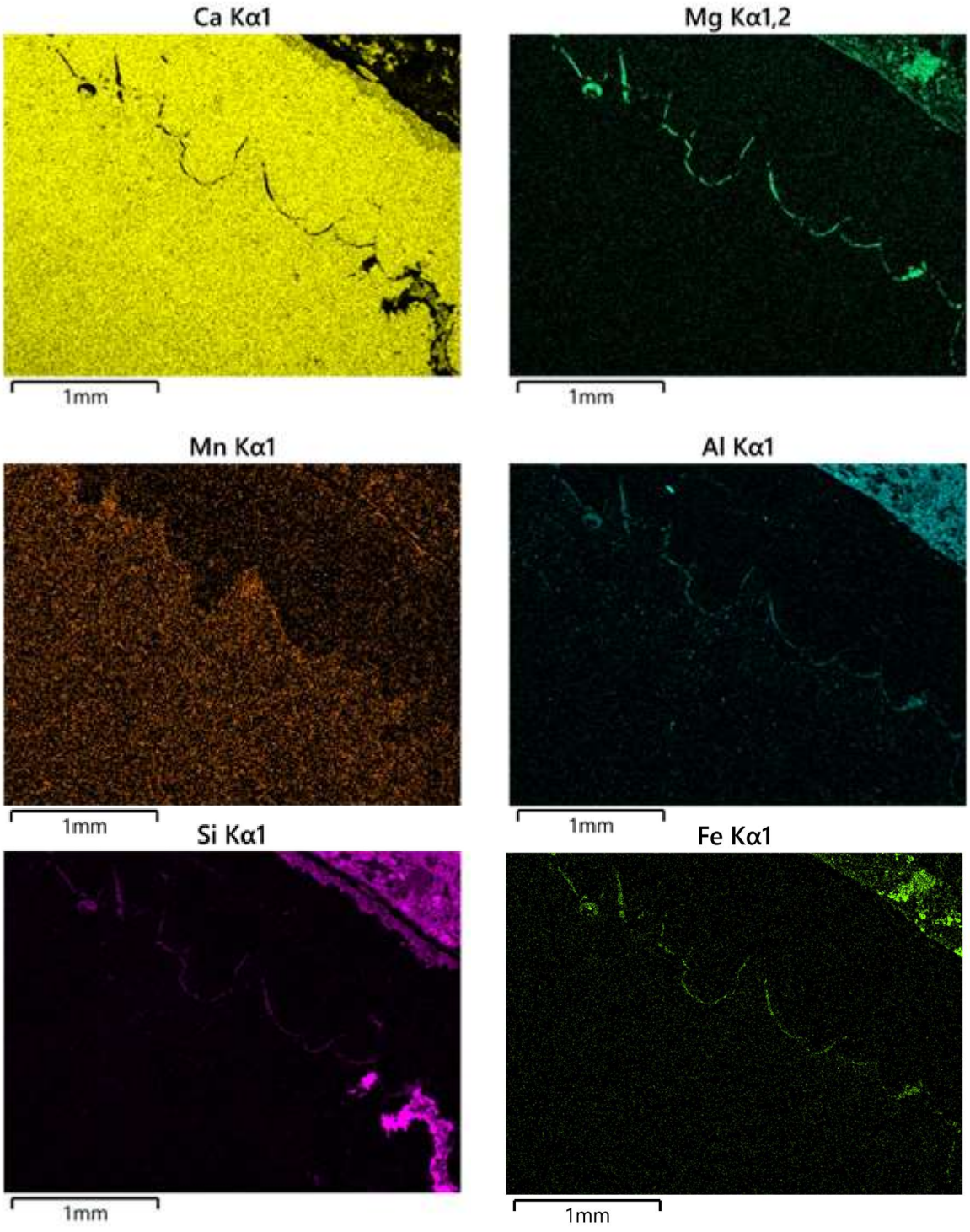

Figure 20. X-Ray maps of sample 28-08-23 1d.

We can see a boundary of Mg and Fe which acts as a barrier for Mn concentrations. This does not impact Ca levels, this can be interpreted as two different phases of growth of calcite, with one having higher Mn and one having lower Mn (Figure 20).

Qualitative Results

Temperature calculation estimates were made using the Mg-in-calcite thermometer from Anovitz and Essene (1986). This calculation uses the mole fraction of $MgCO_3$ as a function of temperature along the solvus (Anovitz & Essene, 1987). The equation used to calculate the estimated temperature is the following:

$$T = A(X_{Cc}^{MgCO_3}) + B/(X_{Cc}^{MgCO_3})^2 + C(X_{Cc}^{MgCO_3})^2 + D(X_{Cc}^{MgCO_3})^{0.5} + E \ (T, \mathrm{K}).$$

(Anovitz & Essene, 1987)

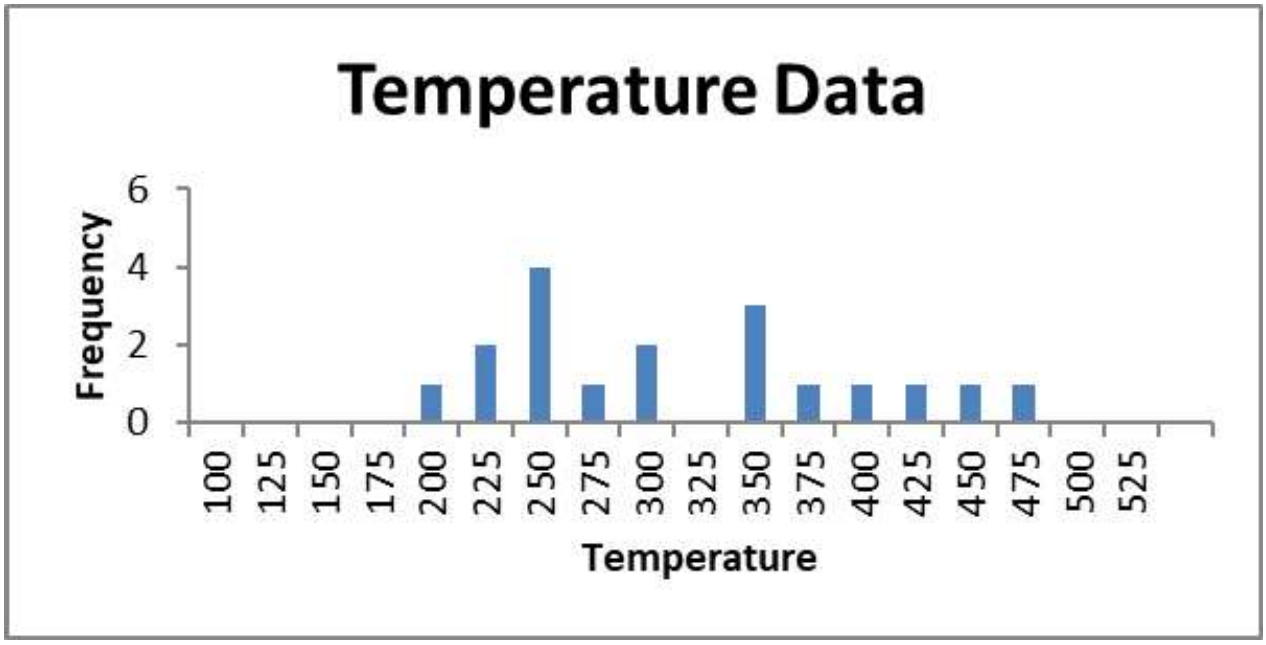

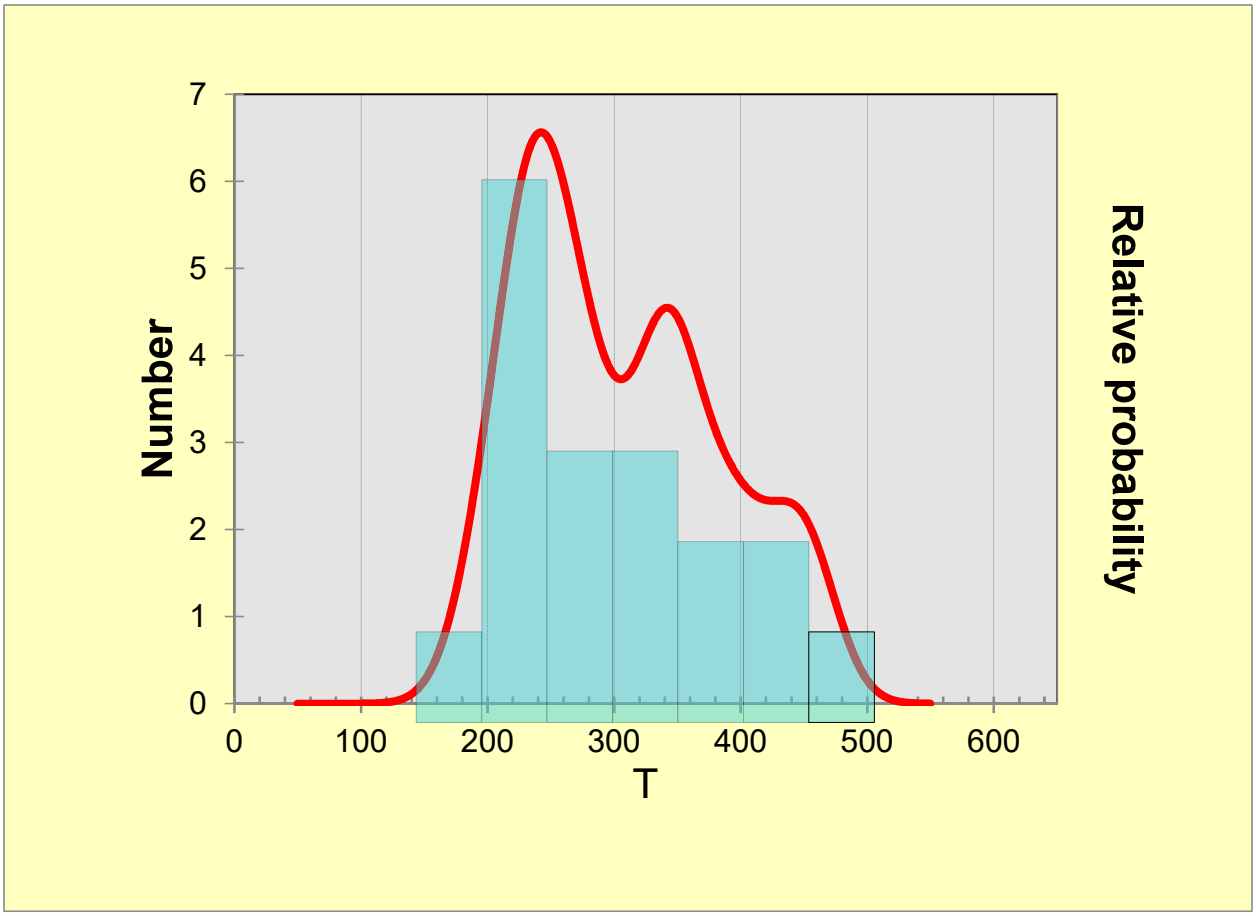

Figure 21. Histograms displaying the calculated temperature estimates from the Mg-in-calcite thermometer, and the weighted mean temperature.

The temperature calculations show two peak temperatures. One around 250°C and one around 375°C. Indicating two growth events. Figure 21b shows the relative probability, which affirms the temperatures seen in the top diagram (Figure 21a)

Using the EDS data a Ca-Mg-Fe ternary plot was made showing the compositions of each sample (Figure 22). The data that plots near Ca is calcite, the data that plots in the middle of the ternary plot is dolomite, and the data that plots on the Mg-Fe axis is ankerite.

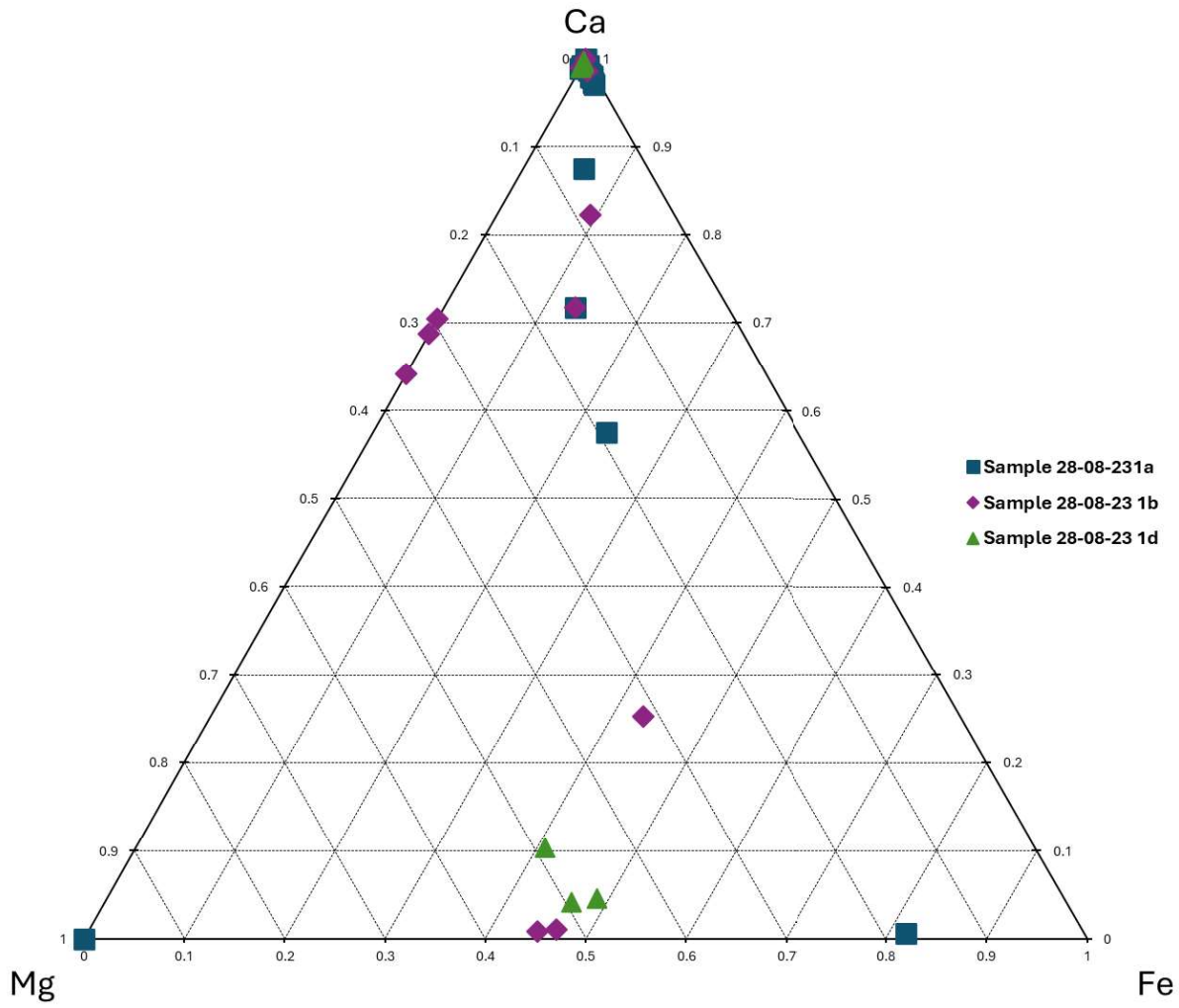

Figure 22. Ternary plot of samples 28-08-23 1a, 28-08-23 1b, and 28-08-23 1d.

The majority of the data points are plotted as calcite, in the top corner of the ternary plot. To further understand this mix, the Fe and Mg data was multiplied by 100, and then the data was renormalized to create a Ca-Mg(x100)-Fe(x100) ternary plot (Figure 23). Figure 23 is helpful to further understand the small compositional differences between the samples, and how those small differences could influence fluorescence.

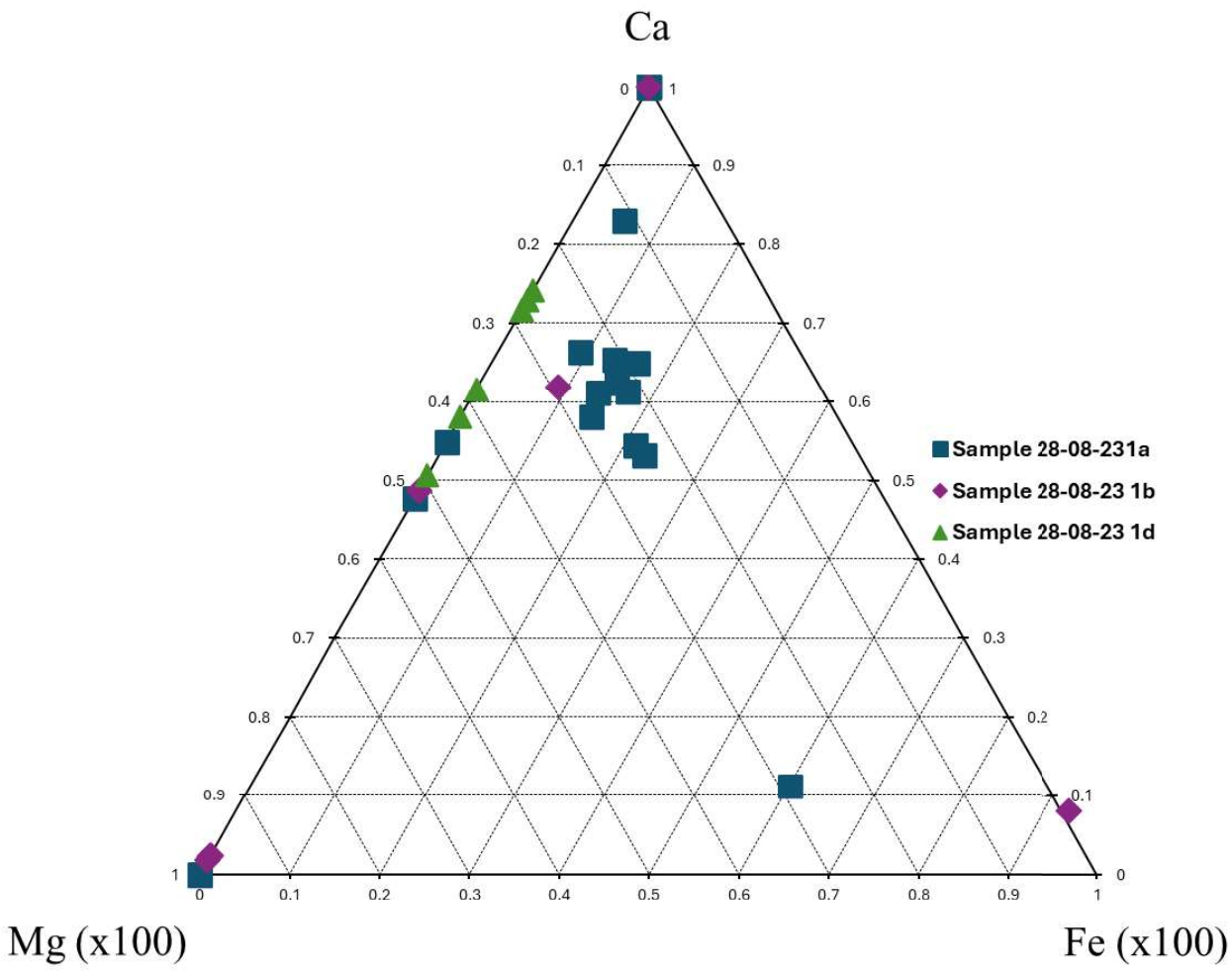

Figure 23. Ternary plot from figure X multiplied Fe and Mg by 100 and re normalized the data This shows the spread within the top 1% of Ca-rich samples.

This shows how sample 1a plots in a cluster, sample 1d has almost no Fe in the calcite, and 1b has a wide range of points. When considering the plotting of sample 1b with the X-ray maps, we see that the irregular nature of the amygdule is shown in both, and there is no clear zoning or compositional consistency.

Chapter 5: Discussion

The Carbonate amygdules are complicated. They are calcite, dolomite, and quartz. There are optical, chemical, and compositional differences within each sample, as well as difference between the samples. In sample 1a the silica layer does not effect the Mn concentration (Figure 8). This silica could be a patch of quartz that formed with the carbonate, with a changing fluid composition. Comparing the incident light photo (Figure 6) to the X-ray maps (Figure 7), the Mn boundary corresponds to an area of grey carbonate. This could indicate a decrease in Mn towards the rim of the amygdule, but it is not concurrent on the other side of the amygdule (top of the amygdule in Figure 7); this could be a form of localized zoning or represent an inconsistency in the fluid composition that firmed the amygdule, possibly it was more Mn rich in one area than another.

The calculated temperatures estimated indicate at least two growth events, a higher temperature event and a lower temperature event (Figure 21). The common temperatures found are relatively low. This low temperature calcite growth makes sense with the carbonate formation proposed by Deer (1967). Possible growth events with these temperatures could be a higher temperature growth from initial post-eruption growth (Rembe et al., 2022), and a lower temperature growth event correlating to the deformation caused by the Acadian Orogeny.

In sample 28-08-23 1b, we continue to see heterogeneous carbonate. Half of the amygdule is green (Figure 10), but this is not explained by the X-ray maps (Figures 14 and 15). There may be another factor causing this that was not measured in this study, but this could be an opportunity for future work. There were only two valid temperature estimates for this sample (Appendix 1). This could be due to an abundance of dolomite in this sample, as the ternary plot shows sample 28-08-23 1b has more dolomite and ankerite than either of the other samples (Figure 22). In the X-ray maps (Figure 15) the dolomite could be formed from exsolution, as the carbonate is irregular and patchy. There are also an abundance of cracks and fractures in the amygdule, which could have caused changes in the composition during growth through the introduction of fluid through these fractures.

In sample 28-08-23 1d there is more clear zoning, which is supported by the incident light images (Figure 17) and the X-ray maps (Figure 20). This shows a decrease in Mn towards the rim, with a boundary of Mg marking where the decrease occurs. There is no visible fracture

or vein that would be a conduit for the Mg rich marker. The silica rich area (bottom right of Figure 20) is curious, and I do not have an explanation. These small silica rich areas are present in each of the sample and can also be seen in the incident light photos. I am unsure if they are from a different fluid composition during mineral formation, or from the basalt and were dislodged and stuck on the amygdule surface during grinding and polishing.

Sample 1d shows lower temperatures in the core (Appendix 1), than the temperature at the rim (Figure 19). Point 10 in 1d shows a temperature of about 200°C, point 7 in 1d shows a temperature of about 400°C (Appendix 1). My interpretation of this is that the rim of the amygdule grew first immediately after eruption, the higher temperature coming from the heat of the basalt. The lower temperature core grew during a secondary deformation event, such as the Acadian orogeny that caused the tilting of the Formation (Murphy, 2001), and the deformation could have caused fluid flow to cause the further calcite growth.

The temperature calculations for sample 1a don't exactly line up to be a higher temperature at the rim than at the core, as they do in sample 1d. This could be due to the growth history being more complicated. There could have been a different influence of deformation on different areas in sample 1a than in 1d, or exsolution of dolomite along the rim of the amygdule to cause lower temperatures.

In terms of fluorescence, Mn being enriched in the core is consistent with studies on Mn as a fluorescent activator (Brown, 1934). A red fluorescence in the core of the amygdule (sample 28-08-23 1d) to a pink layer, then a purple layer where the least Mn concentration was observed. The other elements present could certainly play a role in the fluorescence, as shown in Table 1 there are many elements that contribute to fluorescence that are also present in this study. There is not enough evidence to prove that Mg, Fe, or any of the other elements present are playing a role, but this is another opportunity for future research.

Chapter 6: Conclusion

In conclusion, the carbonate amygdules are a heterogenous mix of calcite, dolomite, and ankerite, with other compositions possible as well. The temperatures found for sample 1a and 1d concur with previous literature on calcite growth (Goldsmith et al., 1955), but sample 1b does not have enough calcite data for accurate temperatures to be reported. This lack of reliable information tell us that the composition of many of the data points were not calcite, therefore reinforcing that more of the amygdules have dolomite or ankerite in them.

For future work, trace elements and rare earth elements can be calculated using an LAICP-MS which can calculate trace elements in parts per million. With the trace and rare earth element composition, the dating using U-Pb can be completed. This will use the isotope compositions to determine the age using the Tera-Wasserberg plot (Tera & Wasserburg, 1972). Final analysis of the results will yield an age for the calcite amygdules, which will relate to the age of the basalts, providing a constraining age for the McArras Brook Formation basalt flows and add to the stratigraphic knowledge of the area. There is also opportunity for future studies on the fluorescence of calcite, to determine a wider range of knowledge of which elements are influencing fluorescence other than Mn.

The relative ages of the carbonate amygdules and veins can be seen, in Figure 21 we see the crosscutting veins with different compositions causing the different coloured fluorescence. The different temperature in the calcite growth indicates different growth events, and relative ages between initial volcanic growth, and deformational growth. The zoning of Mn depleted in the rim and enriched in the core shows that there were different stages of growth, a Mn rich phase and a Mn poor phase. The characterization of these amygdules sets up future work, as the relationship between amygdule and basalt is seen, but further analysis can allow for precise dating.

References

Anovitz, L. M., & Essene, E. J. (1987). Phase Equilibria in the System CaCO3-MgCO3-FeCO3*. *Journal of Petrology*, *28*(2), 389–415. https://doi.org/10.1093/petrology/28.2.389

Bucher, K., & Grapes, R. (2011). Metamorphic Grade. In K. Bucher & R. Grapes (Eds.), *Petrogenesis of Metamorphic Rocks* (pp. 119–187). Springer. https://doi.org/10.1007/978-3-540-74169-5_4

Chave, K. E. (1952). A Solid Solution between Calcite and Dolomite. *The Journal of Geology*, *60*(2), 190–192.

Deer, W. A. et. al.(1967). Rock-Forming Minerals. Vol. 5. Non-Silicates. Longsmans, Green and Coltd.

Dostal, J., Keppie, J. D., & Dupuy, C. (1983). Petrology and geochemistry of Devono-Carboniferous volcanic rocks in Nova Scotia. *Atlantic Geoscience*, *19*(2), Article 2. https://doi.org/10.4138/1566

Frondel, C. and Bauer, L. H. 1955. Kutnahorite: a manganese dolomite, CaMn(CO3)2. Amer. Min., vol. 40, p. 748.

Goldsmith, J. R., & Graf, D. L. (1960). Subsolidus Relations in the System CaCO-MgCO-MnCO. *The Journal of Geology*, *68*(3), 324–335.

Goldsmith, J.R., et. al. (1955). The occurrence of magnesian calcites in nature. *Geochimica et Cosmochimica Acta*, *7*(5), 212–230. https://doi.org/10.1016/0016-7037(55)90033-8

Hermann, J., Troitzsch, U., & Scott, D. (2016). Experimental subsolidus phase relations in the system CaCO3– CaMg(CO3)2 up to 6.5 GPa and implications for subducted marbles.

Contributions to Mineralogy and Petrology, *171*. https://doi.org/10.1007/s00410-016-1296-y

King, H. M. (n.d.). Fluorescent minerals. Fluorescent Minerals. https://geology.com/articles/fluorescent-minerals/

Murphy, J. B. (2001). Geochemistry, provenance, and tectonic significance of sedimentary rocks of the Middle to Late Devonian McArras Brook and Visean Martin Road formations, Merigomish Subbasin, northern Antigonish Highlands, Nova Scotia. *Atlantic Geoscience*, *37*(2/3), Article 2/3. https://doi.org/10.4138/1977

On the geology of Arisaig, Nova Scotia—Image 6—Canadiana. (n.d.). Retrieved October 31, 2023, from https://www.canadiana.ca/view/oocihm.90771/6

Rakovan, J. (2005). Word to the Wise: Amygdule. *Rocks and Minerals*, *80*(3), 202–203.

Rembe, J., et. al. (2022). Calcite U–Pb dating of altered ancient oceanic crust in the North Pamir, Central Asia. *Geochronology*, *4*(1), 227–250. https://doi.org/10.5194/gchron-4-227-2022

Tera, F., & Wasserburg, G. J. (1972). UThPb analyses of soil from the Sea of Fertility. *Earth and Planetary Science Letters*, *13*(2), 457–466. https://doi.org/10.1016/0012-821X(72)90126-4

Appendix A: Composition of carbonate amygdules in samples from McArras Brook Formation, NS. Data obtained using energy dispersive spectroscopy (EDS).

Sample ID	Point	O	Mg	Al	Si	Ca	Mn	Fe	Cl	Ti	K	Na	S	Ba	Sb	Total	Estimated T (°C)
28-08-23 1a	1	28.56	0.56		0.23	68.18	2.47									100	402.371
28-08-23 1a	2	36.52	0.41	0.6	14.98	37.48	1.53						1.63	6.86		100	455.415
28-08-23 1a	3	50.85			42.2	6.96										100	-
28-08-23 1a	4	40	6.61	7.98	15.62	19.82	1.87	8.03				0.08				100	-
28-08-23 1a	5	51.64			43.72	4.43	0.22									100	-
28-08-23 1a	7	28.44	0.27		0.12	68.53	1.71	0.94								100	238.793
28-08-23 1a	8	28.69	0.1	0.45	0.32	68.13	1.93	0.4								100	-
28-08-23 1a	9	28.33	0.28		0.07	67.54	3.15	0.63								100	249.612
28-08-23 1a	10	28.79	0.3	0.65	0.36	67.16	1.76	1.04								100	272.255
28-08-23 1a	11	28.42	0.43		0.26	66.65	2.66	1.57								100	351.433
28-08-23 1a	12	28.47	0.39		0.19	67.92	2.02	1.01								100	329.853
28-08-23 1a	13	28.76	0.25	0.3	0.64	66.79	2.15	1.11								100	221.538
28-08-23 1a	14	28.53	0.31	0.22	0.2	67.72	1.83	1.18								100	277.723
28-08-23 1a	15	28.38	0.34			68.57	1.75	0.96								100	297.866

28-08-23		28.6				66.2	2.3									
1a	16	9	0.41	0.49	0.39	3	4	1.45							100	343.836
28-08-23		37.6			17.2	43.5	1.2									
1a	17	5		0.22	8	7	8								100	-
28-08-23		50.9		12.2	34.7				0.9							
1a	18	3		3	5	1.15			3						100	-
28-08-23				12.5	29.0						2.2	4.5				
1a	19	47.8		1	6	3.8					6	6			100	-
28-08-23		35.7					1.1	35.1		1.5						
1a	20	6	7.6	7.52	11	0.28	6	5		2					100	-
28-08-23					46.4											
1a	21	53.2	0.17	0.15	8										100	-
28-08-23		31.5				52.4										
1a	22	9	3.84	2.28	3.84	5	2.4	3.6							100	-
28-08-23		35.7				34.2	2.5									
1a	23	4	7.22	4.78	9.26	3	2	6.24							100	-
28-08-23		52.8			45.7				0.1							
1b	1	6	0.25	0.42	7	0.2		0.34	6						100	-
28-08-23		42.7	15.5		17.5		0.9	13.7								
1b	2	1	5	9.08	9	0.29	9	9							100	-
28-08-23		33.1				44.5	2.7									
1b	3	6	4.58	4.7	5.21	6	7	5.03							100	-
28-08-23		52.9			46.1				0.3			0.1				
1b	5	2		0.24	6	0.15			5			7			100	-
28-08-23		43.1	15.8		18.1		0.5	13.0								
1b	6	1	9	8.96	5	0.25	9	5							100	-
28-08-23		28.3				68.4	2.1									
1b	7	8	0.36			8	7	0.62							100	311.075
28-08-23						68.4								2.5		
1b	8	28.3	0.72			5								4	100	453.578
28-08-23		32.8	23.2			41.6								1.7		
1b	9	3	6		0.47	8								6	100	-
28-08-23		31.8	19.4			46.5								2.1		
1b	10	3	9			5								3	100	-

28-08-23		31.9	20.7					1.4					
1b	11	6	9			45.8		5				100	-
28-08-23		28.6				70.8							
1d	1	8	0.28		0.18	6						100	247.381
28-08-23		33.3				53.7	3.1						
1d	2	1	0.2	0.68	8.96	1	3					100	217.852
28-08-23					35.9		0.5						
1d	3	49.7	4.09	5.06	6	0.4	1	4.28				100	-
28-08-23		28.1				65.5	5.8						
1d	4	5	0.41			8	6					100	341.210
28-08-23		30.6				63.5							
1d	5	5	0.46	4.56	0.82	1						100	383.288
28-08-23		28.3				68.0	3.3						
1d	6	2	0.27			7	4					100	238.542
28-08-23		28.6				70.6							
1d	7	6	0.69			5						100	439.755
28-08-23					34.3		0.6						
1d	8	49.2	4.95	5.69	9	0.42	8	4.67				100	-
28-08-23		43.7	11.6	14.1	16.9		1.3						
1d	9	2	9	3	3	2.48	1	9.73				100	-
28-08-23						66.0	4.4						
1d	10	28.6	0.23		0.7	2	6					100	194.331